

AD-A077 028 ILLINOIS UNIV AT URBANA-CHAMPAIGN DEPT OF ELECTRICAL --ETC F/G 4/1  
MODEL COMPUTATIONS OF RADIO WAVE SCINTILLATION CAUSED BY EQUATO--ETC(U)  
JUL 79 A W WERNIK F19628-78-C-0195  
UNCLASSIFIED UIIU-ENG-79-2555 AFGL-TR-79-0165 NL

ILLINOIS UNIV AT URBANA-CHAMPAIGN DEPT OF ELECTRICAL --ETC F/G 4/1  
MODEL COMPUTATIONS OF RADIO WAVE SCINTILLATION CAUSED BY EQUATO--ETC(U)  
JUL 79 A W WERNIK F19628-78-C-0195  
UILLU-ENG-79-2555 AFGL-TR-79-0165 NL

UNCLASSIFIED

AFGL-TR-79-0165

NL

1 OF 1  
AD-  
A077028



END  
DATE  
FILMED  
2-79  
DDC

AFGL-TR-79-0165

**LEVEL**

12

**MODEL COMPUTATIONS OF RADIO WAVE SCINTILLATION  
CAUSED BY EQUATORIAL BUBBLES**

A. W. Wernik

Department of Electrical Engineering  
University of Illinois at Urbana-Champaign  
Urbana, Illinois 61801

July 1979

Scientific Report, No. 1

DDC  
REFILED  
NOV 21 1979  
RECEIVED  
E

Approved for public release; distribution unlimited.

AD A 077 028

DDC FILE COPY

AIR FORCE GEOPHYSICS LABORATORY  
AIR FORCE SYSTEMS COMMAND  
UNITED STATES AIR FORCE  
HANSCOM AFB, MASSACHUSETTS 01731

79 19 9 140

Qualified requestors may obtain additional copies from the Defense Documentation Center. All others should apply to the National Technical Information Service.

UNCLASSIFIED

SECURITY CLASSIFICATION OF THIS PAGE (When Data Entered)

19 REPORT DOCUMENTATION PAGE		READ INSTRUCTIONS BEFORE COMPLETING FORM	
1. REPORT NUMBER (18) AFGL TR-79-0165	2. GOVT ACCESSION NO.	3. RECIPIENT'S CATALOG NUMBER	
4. TITLE (and Subtitle) (6) Model Computations of Radio Wave Scintillation Caused by Equatorial Bubbles		5. TYPE OF REPORT & PERIOD COVERED No. 1 Scientific, July 1978 through July, 1979	
7. AUTHOR (10) A. W. Wernik		6. PERFORMING ORG. REPORT NUMBER TR No. 64, UILU-ENG-79-2555	
9. PERFORMING ORGANIZATION NAME AND ADDRESS Department of Electrical Engineering University of Illinois at Urbana-Champaign Urbana, Illinois 61801		8. CONTRACT OR GRANT NUMBER(s) (15) F19628-78-C-0195	
11. CONTROLLING OFFICE NAME AND ADDRESS Air Force Geophysics Laboratory (PHP) Hanscom AFB, Massachusetts 01731 Monitor/Herbert E. Whitney/PHP		10. PROGRAM ELEMENT, PROJECT, TASK AREA & WORK UNIT NUMBERS (16) 63431F 464305AA (17) 052	
14. MONITORING AGENCY NAME & ADDRESS (if different from Controlling Office)		12. REPORT DATE (11) Jul 79	
		13. SECURITY CLASS. (of this report) UNCLASSIFIED	
		15A. DECLASSIFICATION/DOWNGRADING SCHEDULE	
16. DISTRIBUTION STATEMENT (of this Report)  Approved for public release; distribution unlimited.			
17. DISTRIBUTION STATEMENT (of the abstract entered in Block 20, if different from Report) (14) UILU-ENG-79-2555, TR-64			
18. SUPPLEMENTARY NOTES (9) Scientific rept. no. 1, Jul 78-Jul 79,			
19. KEY WORDS (Continue on reverse side if necessary and identify by block number)  Equatorial scintillation Ionosphere bubbles Gigahertz scintillation Parabolic equation			
20. ABSTRACT (Continue on reverse side if necessary and identify by block number)  The apparent inhomogeneous nature of the equatorial electron density irregularities indicate that a new approach to the scintillation theory is required. Based on the available in situ electron density measurements and theoretical information a simple two-dimensional, deterministic model of the equatorial bubble is developed. The parabolic equation for a wave traversing such a bubble is solved numerically. The computed amplitude pattern suggests that wave diffraction on edges formed by sharp horizontal electron density gradients may be a possible cause of scintillation at gigahertz frequencies. Comparison with the			

DD FORM 1473

EDITION OF 1 NOV 65 IS OBSOLETE

UNCLASSIFIED

276 009

xlt

20. Cont.

results obtained for a model of random irregularities with the same power spectrum shows that the medium characterized by sharp electron density gradients leads to stronger scintillation in a wide frequency range.

The amplitude pattern, scintillation index, frequency dependence and scatter plots computed for the model agree well with observations.

# TABLE OF CONTENTS

	Page
1. INTRODUCTION . . . . .	1
2. SUMMARY OF CURRENT EXPERIMENTAL AND THEORETICAL UNDERSTANDING OF EQUATORIAL IRREGULARITIES . . . . .	3
3. BASIS OF THE SCINTILLATION MODEL . . . . .	8
3.1 Parabolic Equation. . . . .	8
3.2 Irregularity Model. . . . .	12
4. NUMERICAL METHOD FOR SOLVING PARABOLIC EQUATION. .	15
5. NUMERICAL RESULTS AND DISCUSSION . . . . .	20
6. CONCLUSIONS. . . . .	31
REFERENCES. . . . .	33
APPENDIX. . . . .	36

Accession For	
NTIS GRA&I	<input checked="checked" type="checkbox"/>
DDC TAB	<input type="checkbox"/>
Unannounced	<input type="checkbox"/>
Justification	
By _____	
Distribution/ _____	
Availability Codes	
Dist <input checked="checked" type="checkbox"/>	Avail and/or special

## TABLE OF CONTENTS

	Page
1. INTRODUCTION . . . . .	1
2. SUMMARY OF CURRENT EXPERIMENTAL AND THEORETICAL UNDERSTANDING OF EQUATORIAL IRREGULARITIES . . . . .	3
3. BASIS OF THE SCINTILLATION MODEL . . . . .	8
3.1 Parabolic Equation. . . . .	8
3.2 Irregularity Model. . . . .	12
4. NUMERICAL METHOD FOR SOLVING PARABOLIC EQUATION. .	15
5. NUMERICAL RESULTS AND DISCUSSION . . . . .	20
6. CONCLUSIONS. . . . .	31
REFERENCES. . . . .	33
APPENDIX. . . . .	36

## 1. INTRODUCTION

Recent activity in the equatorial scintillation studies was enhanced by the discovery of scintillating gigahertz frequency radio signals (Skinner et al., 1971) and by the new and fascinating experimental and theoretical results for the irregular structure of the equatorial ionosphere. Several papers reviewing equatorial scintillation phenomena and theory and measurements of equatorial irregularities were published recently by Farley et al., (1970); Basu and Kelley, (1977); Basu and Kelley (1979); Ossakow et al., (1979)). Interested readers should refer to these papers for more detailed references. In Section 2 only a brief summary of results pertinent to the future discussion is given. As will become evident, equatorial irregular structure can not be considered as random, mainly because of the presence of sharp gradients of electron concentration. Under such circumstances, a deterministic approach to scintillation is certainly more correct. The approach used in this report is based on the assumption of validity of the parabolic equation describing the complex wave amplitude for a wave propagating in a model irregular ionosphere. The model, which is deterministic, is based on the available satellite in-situ data and other experimental and theoretical information. It is described in Section 3. Section 4 and the Appendix discuss the numerical method, algorithm and computer program used to solve most efficiently the parabolic equation.

As shown in Section 5, modelling proved clearly the importance of the presence of sharp horizontal electron concentration gradients in producing strong scintillation of gigahertz frequency radio waves. Although the model is deterministic, some statistical parameters of radio waves have been computed, and frequency dependence of the scintillation index was found to be in good agreement with observations.

## 2. SUMMARY OF CURRENT EXPERIMENTAL AND THEORETICAL UNDERSTANDING OF EQUATORIAL IRREGULARITIES

Most information about the irregular structure of the equatorial ionosphere has come from back-scatter radar and in-situ satellite and rocket measurements. Several campaigns of simultaneous measurements of different types provided deeper insight into the nature of equatorial irregularities. Jicamarca back-scatter radar data show that 3-m size irregularities initially, right after sunset, occupy relatively thin layers below the F-layer peak which rapidly, sometimes in a matter of several minutes, thickens to several hundred kilometers extending well above the F-peak (Farley et al., 1970; Woodman and La Hoz, 1976). The extended irregular structures are called "plumes," which usually move with the velocity of the order of  $100 \text{ ms}^{-1}$ , occasionally exceeding  $300 \text{ ms}^{-1}$ . Simultaneous VHF scintillation measurements (Basu et al., 1977) show that as long as the irregular layer is thin scintillation intensity is low or moderate and the fading rate is small. However, the stage of fully developed plumes is accompanied by intense ( $>20\text{dB}$  on VHF) and rapid scintillation. At times of intense VHF scintillation, gigahertz frequency radio signals also scintillate. This scintillation is unexpectedly strong, exceeding 8 dB at 1.5 GHz and 4 dB at 4 GHz. Scintillation indices as large as 0.74 at 1.5 GHz and 0.63 at 4 GHz were reported (Taur, 1976). Evidently, in such cases, the weak scattering scintillation theory is not valid. Discussion of possible

causes of strong gigahertz frequency scintillation is one of the objects of this report.

It has been pointed out (Basu et al., 1978) that 3-m and km-size irregularities responsible for VHF scintillation coexisted only in the developing stage of plume, and in the later evening hours scintillation did not correlate with plumes. This led Basu et al. to speculate about the change of the cut-off scale size of the irregularity spectrum.

In-situ rocket and satellite measurements provided further information about equatorial irregularities. OGO-6 data showed that irregularities are usually associated with large depletions of the electron concentration known as bubbles (McClure et al., 1977). These bubbles move upward and westward with the velocity of the order of  $150 \text{ ms}^{-1}$  with respect to the background plasma (which at night rotates eastward). The observed east-west size of the bubbles ranges from 10 to several hundred kilometers and the depletions in bubbles up to three orders of magnitude were observed. Figure 1 illustrates the irregular structure inside the bubble. The very sharp gradients and the peaks are the most striking features. Similar structures have been observed below the F-peak during the rocket flights (Costa and Kelley, 1978). Costa and Kelley (1978) have shown that these kinds of structures have a one-dimensional power spectrum of the form  $k^{-2}$ , resembling the spectrum of turbulent-like irregularities. From the point of view of the scintillation theory, this is a very important result. The irregularity power spectrum plays a very important role in

the statistical theory of scintillation which makes use of the statistical properties of a medium to derive statistics of a scintillating wave. It is assumed that the irregularities are random and the background medium is homogeneous, or at least locally homogeneous. However, in the presence of sharp electron concentration gradients none of these two assumptions are exactly valid, and the scintillation theory based on other models may be more appropriate for the situation. Furthermore, mechanisms other than scattering and diffraction have been suggested to be efficient in producing scintillation (Crain et al., 1979). This point is discussed in more detail later on.

Recent simultaneous total electron content, airglow, and scintillation measurements provided further evidence that irregularities responsible for scintillation are associated with depletions in electron concentration (Koster, 1976; Weber et al., 1978; Yeh et al., 1979). This association is especially clear in the premidnight period.

Theoreticians were very successful in explaining the observed irregular structure of the equatorial ionosphere. The hierarchy of plasma instabilities suggested by Haerendel (1974) could produce a wide spectrum of observed irregularities. First in the hierarchy is the collisional Rayleigh-Taylor instability, which acts on the steep bottomside gradient of electron concentration and produces large-scale vertically oriented irregularities with sharp horizontal gradients. Favorable conditions for the cross-field instability are

created. This kind of instability leads to irregularities with wave-vectors oriented vertically and sizes roughly between 0.5 to 5 km. When the amplitude of these irregularities is large enough, the collisionless Rayleigh-Taylor instability becomes active and produces irregularities with sizes 50 to 500 m. Finally, kinetic drift waves can grow upon these irregularities after they reach large amplitudes. Irregularities generated by this mechanism will have sizes comparable to the ion gyro-radius (several meters).

Numerical simulation of the collisional Rayleigh-Taylor instability (c.f. Scannapieco and Ossakow, 1976; Ossakow et al., 1979) showed that originally bottomside plasma depletions can rise beyond the F peak. Figure 2 from Ossakow et al. (1979) shows the evolution of a bubble. Percentage depletion as large as 85% was reached and the rise velocity of the bubble was  $160 \text{ ms}^{-1}$ . Note the sharp electron concentration gradient on the leading edge of the bubble. An analytical model of uprising bubbles has been developed by Ott (1978) in the collision-dominated and the collisionless cases. Kelley and Ott (1978) showed that rising bubbles generate a wake with vortices. Originally, such vortices have a characteristic size of the order of the bubble size. In the presence of the background plasma density, gradient vortices will mix regions of differing density and create density irregularities with wavelengths both larger and smaller than the original size of the bubble. The power spectrum of density irregularities will be

proportional to  $k^{-1}$  for irregularities with sizes between the bubble size and the dissipation scale ( $\approx 28$  m for the case considered by Kelley and Ott). This seems to contradict the observed  $k^{-2}$  spectrum but, as pointed out by the authors, steepening of the spectrum is most likely due to the sharp edges of bubbles.

### 3. BASIS OF THE SCINTILLATION MODEL

The scintillation theory relates statistics of the wave parameters to statistics of the dielectric permittivity fluctuations  $\epsilon_1$  and, therefore, of electron concentration fluctuations. If dielectric permittivity fluctuations  $\epsilon_1(\vec{r}, z)$  can be considered as a Gaussian random field, then statistics of  $\epsilon_1$ , and therefore of the complex amplitude, are completely determined by the first two moments of the field: its mean and autocorrelation function or structure function. If it is further assumed that the field is homogeneous, instead of the autocorrelation or structure function, the power spectrum can be used. This assumption is always made in the scintillation theory. It prevents us from considering the fields of  $\epsilon_1$  with sharp gradients, because in this case,  $\epsilon_1$  is certainly inhomogeneous. On the other hand, sharp electron concentration gradients are the most pronounced features of the irregular equatorial ionosphere. Consequently, some new approach to the scintillation is needed. In addition to that, sharp discontinuities in  $\epsilon_1$  can produce qualitatively new effects leading to scintillation (Crain et al., 1979).

In the rest of this section, the basis for the scintillation model free from assumptions on statistics of  $\epsilon_1$  is developed.

#### 3.1 Parabolic Equation

A starting point for our consideration is the so-called parabolic equation (cf. Tatarski, 1971). For a wave propagating

in the  $z$  direction, it takes the form

$$-2ik \frac{\partial u}{\partial z} + \nabla_T^2 u + k^2 \epsilon_1 u = 0 \quad (3.1)$$

where  $u$  is the complex wave amplitude,  $\epsilon_1 = \epsilon - \langle \epsilon \rangle$  is the dielectric permittivity variation relative to some reference value  $\langle \epsilon \rangle$ ,  $\nabla_T^2$  is the transverse to the direction of propagation part of the Laplacian operator, and  $k = 2\pi/\lambda$  is the wave number in the reference medium.

To apply (3.1) it is required (Tatarski, 1971) that:

- (A) the characteristic scale of  $\epsilon_1$  variations is much larger than the wavelength.
- (B) wave attenuation due to the presence of irregularities is small over a distance equal to the wavelength.

In addition, two sufficient conditions must be satisfied:

- (C) the power reflected back is negligible,
- (D) the Fresnel approximation is valid.

If conditions (A) - (D) are satisfied, equation (3.1) can be used in any medium, stochastic or deterministic. In the stochastic medium, the reference dielectric permittivity is simply the average value, while in the deterministic medium it can be any value. In our calculations  $\langle \epsilon \rangle$  has been chosen to be equal to 1, which is the value  $\epsilon$  assumes outside the irregular region.

Condition (A) requires  $l = \epsilon_1 (\nabla \epsilon_1)^{-1}$  to be much larger than the wavelength. Condition (D) is satisfied whenever (cf. Tatarski, 1971)

$$\frac{L}{k^3 l^4} \ll 1, \quad (3.2)$$

and, if only  $kl \ll 1$ , this inequality is valid even in the far zone where a distance  $L$  traversed by a wave is larger than  $(kl)^{1/2}$ .

Conditions (B) and (C) are much more difficult to discuss. To have some impression about the order of magnitude of wave attenuation in a deterministic medium, consider the case when  $\epsilon_1$  is a Gaussian function of  $x$  and  $y$

$$\epsilon_1(x, y) = \epsilon_{10} \exp(-\rho^2/r^2) \quad \bar{\rho} = (x, y) \quad (3.3)$$

and this irregularity extends throughout a distance  $L$  in the direction of propagation. Most of the attenuation results from the single scattering, therefore, if the power extracted from the incident wave by single scattering is small over a distance equal to the wavelength, the condition (B) is satisfied. Assuming that the Fresnel approximation is valid, a single scattered wave field is given by the equation:

$$u_1(\bar{\rho}, L) = \frac{k^2 u_0}{4\pi} \int_0^L \frac{dz'}{L-z'} \iint_{-\infty}^{\infty} \epsilon_1(\bar{\rho}', z') \exp\left[-\frac{ik(\bar{\rho}-\bar{\rho}')}{2(L-z')}\right] d\bar{\rho}' \quad (3.4)$$

where  $u_0$  is constant for a plane incident wave. For simplicity, we set  $\bar{\rho}=0$ , therefore, the upper estimate of the scattered power is obtained. Substituting (3.3) into (3.4), integrating and taking the absolute value of  $u_1$  leads to the result

$$\frac{|u_1|^2}{u_0^2} = \frac{k^4 r^4 \epsilon_{10}^2}{16} (\ln^2 \rho + \phi^2), \quad (3.5)$$

$$\rho^2 = 1 + (2L/r^2 k)^2, \quad \phi = \arctan(2L/r^2 k),$$

which is the fraction of the incident power attributed to a single scattering. The inverse of the extinction length  $d$  is obtained by dividing (3.5) by the slab thickness  $L$ . Extinction length is a measure of the wave attenuation. If  $d^{-1}/k \ll 1$  condition (B) is satisfied.

Consider first the case  $2L/kr^2 \ll 1$ . It is easy to show that in this case

$$d^{-1}/k \approx kL\epsilon_{10}^2/4. \quad (3.6)$$

If (3.6) is multiplied and divided by  $2kr^2$ , the condition (B) can be written in the following form

$$\frac{k^2 r^2 \epsilon_{10}^2}{8} \frac{2L}{kr^2} \ll 1. \quad (3.7)$$

Note that an irregularity of size  $r$  causes the phase change  $kr\epsilon_{10}/2$ . Therefore, inequality (3.7) means that for  $2L/kr^2 \ll 1$ , the condition (B) is satisfied even for large phase variations introduced by a single irregularity.

For  $2L/kr^2 \gg 1$  the value of  $d^{-1}/k$  can be approximated by the following expression:

$$d^{-1}/k \approx \frac{k^4 r^4 \epsilon_{10}^2}{4} [\ln(2L/kr^2)]^2 = k^2 L^2 \epsilon_{10}^2 \left[ \frac{\ln(2L/kr^2)}{2L/kr^2} \right]^2 \quad (3.8)$$

and the condition  $d^{-1}/k \ll 1$  means that the total phase change  $kL\epsilon_{10}$  can not be exceedingly large.

To discuss condition (C) again, assume the Gaussian irregularity. One can expect that, whenever the scattering angle is small not too much power is reflected back. To estimate the scattering angle note that in the plane  $y=\text{const}$  it can be expressed in terms of the phase  $\phi$  by

$$\alpha = \frac{1}{k} \frac{\partial \phi}{\partial x} \quad (3.9)$$

where  $\phi = k\epsilon_1 L/2$ . In our irregularity model, the scattering angle is maximum for  $y=0$  and  $x=r/\sqrt{2}$ , where it assumes the value

$$\alpha_{\max} = 0.46 \frac{L\epsilon_{10}}{r} = 0.46 \frac{kL\epsilon_{10}}{kr} \quad (3.10)$$

Condition (C) is satisfied provided  $\alpha_{\max} \ll 1$ . It is clearly seen from (3.10) that with  $kr \gg 1$  this puts a limit on the total phase change.

With strong irregularities filling up the extended bubble structures, assumptions leading to the parabolic equation could be violated especially at lower frequencies. In fact, condition (B) is violated in our model calculations when scintillation at a frequency of 136 MHz is considered to be due to irregularities at the center of the well-developed bubble (Section 3.2). A rough estimate shows that in this case  $d^{-1}/k$  is larger than one for irregularities with the scale size smaller than 200 m.

### 3.2 Irregularity model

A parabolic equation can be solved numerically only if  $\epsilon_1(\vec{r}, z)$  is known at each point of a three-dimensional space.

Because of the direct proportionality to electron concentration fluctuations  $\Delta N$ ,  $\epsilon_1$  can be determined provided  $\Delta N$  is known from measurements. Unfortunately, satellite and rocket in-situ measurements give information only about  $\Delta N$  along the satellite (rocket) path. Any attempt to obtain from these data a three-dimensional structure of irregularities would involve assumptions about their statistics. This is feasible if the data show randomness of  $\Delta N$ . Figure 1 clearly shows that this is not the case: in addition to the large scale trend, sharp gradients of  $\Delta N$  are present inside the bubble.

The two-dimensional model adopted for our calculation is very simple. It is assumed that at each height the horizontal relative variations of electron concentration  $\Delta N/N$  are the same as those displayed in Figure 1. The concentration at the bubble's edge is taken as a reference. Allowance is made for its variations with the height and, in particular, the parabolic profile is adopted.

$$N(h) = N_0 [1 - (h - h_0)^2 / H^2] \quad (3.2.1)$$

where  $N_0$  is the maximum electron concentration at the height  $h_0$  and  $H$  is the scale height. In most cases we set  $h_0 = 350$  km,  $N_0 = 2.5 \cdot 10^5$  electrons  $\text{cm}^{-3}$  and  $H = 110$  km.

As was noticed in Section 2 theoretical simulations show that in the course of the bubble development its leading edge becomes sharper while the trailing edge seems

to be more blunt. To take this into account (3.2.1) is multiplied by some weighting function. The weighting function corresponding to what we call initial stage is shown in Figure 3a, while Figure 3b displays the weighting function for the developed stage of the bubble.

The model, is summarized in Figures 4a and 4b, which show electron concentration variations  $\Delta N$  at several levels inside the bubble for the initial and developed stages, respectively.

Our model is far from being perfect. In particular it does not take into account small-scale vertical variations of the electron concentration. But at least it is free from any assumptions about the statistics of  $\Delta N$  and should correctly answer the question about the role of vertically extended sharp gradients in producing scintillation.

#### 4. NUMERICAL METHOD FOR SOLVING PARABOLIC EQUATION

The parabolic equation (3.1) can be solved analytically only for a very few simple forms of the function  $\epsilon_1(\bar{\rho}, z)$ . A general numerical approach is needed. We are interested in solving (3.1) when the dielectric permittivity is a function of  $x$  and  $z$  only, thus,  $\nabla_T^2 = \partial^2 / \partial x^2$ . For a plane incident wave the initial value for this equation is  $u(x, 0) = \text{const} = 1$ . The change of variables  $t = kz$ ,  $\xi = kx$  leads to the equation

$$\frac{\partial u}{\partial t} + \frac{i}{2} \frac{\partial^2 u}{\partial \xi^2} + \frac{i}{2} \epsilon_1(\xi, t) u = 0 \quad (4.1)$$

Basically, two methods for the numerical treatment of parabolic equations exist: explicit and implicit method (cf. Ames, 1969). Although the explicit method is very simple and does not involve the troublesome solution of a large set of equations, it gives a somewhat imperfect model for a parabolic equation (Ames, 1969), and places a stringent restriction on the step-size in the  $t$ -direction. Because of this, we have chosen as an implicit scheme a special case which is the well-known Crank-Nicholson difference scheme. A thorough discussion of the stability condition, truncation error and convergence has been made by Crandall (1955) (see also Ames, 1969) for the diffusion equation and for a special case of the equation analogous to (4.1) by Borodziewicz (1978). The scheme makes use of the following analog to the second derivative:

40

$$\frac{\partial^2 u}{\partial \xi^2} = \frac{1}{h^2} [\sigma (u_{k+1}^{n+1} - 2u_k^{n+1} + u_{k-1}^{n+1}) + (1-\sigma) (u_{k+1}^n - 2u_k^n + u_{k-1}^n)], \quad (4.2)$$

where  $u_k^n = u(kh, n\tau)$  with  $h$  and  $\tau$  being the step sizes in the  $\xi$  and  $t$  directions, respectively, and  $0 \leq \sigma \leq 1$  is a weighting factor. The term  $\partial u / \partial t$  is approximated by

$$(u_k^{n+1} - u_k^n) / \tau, \quad (4.3)$$

and the term  $c_1 u$  by

$$\frac{c_{1k}^{n+1} + c_{1k}^n}{2} [\sigma u_k^{n+1} + (1-\sigma) u_k^n]. \quad (4.4)$$

If  $\sigma=0$  the explicit scheme is obtained, while  $\sigma=1/2$  results in the Crank-Nicholson scheme. In general, increased  $\sigma$  improves stability and convergence of the solution for a given value of  $r=\tau/h^2$ . If  $\sigma \geq 1/2$ , the solution is absolutely stable for all  $\tau$ , and if  $\sigma=1$ , the solution is absolutely stable and convergent. For the heat transfer equation, a minimum truncation error of the order of  $O(h^4)$  is attained for

$$r = \frac{1}{\sigma(1-2\sigma)}. \quad (4.5)$$

Otherwise, the truncation error is of the order of  $O(h^2)$ .

We see that the Crank-Nicholson scheme requires an infinitely large value of  $r$  to reach minimum error. For equation (4.1)

no corresponding relation was derived. However, computer runs showed that a satisfactory compromise between the error and convergence is attained if  $\sigma=0.51$  and  $0.5 < r < 2.5$ .

Substitution of (4.2), (4.3) and (4.4) into the parabolic equation (4.1) leads to the following difference equation:

$$\begin{aligned} \frac{i\tau}{2h^2} \sigma u_{k+1}^{n+1} + (1 - \frac{i\tau}{h^2} \sigma + \frac{i\tau}{2} \sigma f_k^n) u_k^{n+1} + \frac{i\tau}{2h^2} \sigma u_{k-1}^{n+1} = \\ - \frac{i\tau}{h^2} (1-\sigma) u_{k+1}^n + [1 + \frac{i\tau}{h^2} (1-\sigma) - \frac{i\tau}{2} (1-\sigma) f_k^n] u_k^n \\ - \frac{i\tau}{2h^2} (1-\sigma) u_{k-1}^n, \end{aligned} \quad (4.6)$$

$$k = \underline{+1}, \underline{+2}, \dots, \underline{+K}$$

$$n = 0, 1, 2, \dots, N$$

where  $f_k^n = (\epsilon_{1k}^{n+1} + \epsilon_{1k}^n)/2$ .

In the discrete scheme the initial value  $u(x,0)=1$  is written  $u_k^0=1$ . Because of the assumed symmetry of  $\epsilon_1(x,z)$  with respect to the  $z$  axis,  $u_{-k}^n = u_k^n$ , and the system (4.6) of  $2K$  equations reduced to the system of  $K$  equations. It contains  $K+2$  unknowns  $u_k^n$  with  $K$  unknowns of interest to us ( $k=1,2, \dots, K$ ), and two unknowns  $u_0^n$  and  $u_{K+1}^n$  beyond the boundaries of the considered region. The usual procedure is to introduce the so-called "false" boundaries at  $k=0$  and  $k=K+1$ . If the derivatives of  $u$  at the "true" boundaries are known these "false" boundaries can be easily derived.

We set  $u_0^n = 0$  and  $u_{k+1}^n = 0$  which introduces some discontinuities. As noticed by Ames (1969), if the stable scheme is used, the effect of such discontinuities does not penetrate deeply into the field of integration. In this way, the system (4.6) becomes tridiagonal with  $K$  unknowns. It can be written in the matrix form

$$B^n U^{n+1} = (B^n - \tau A^n) U^n, \quad n=0,1,2,\dots,N \quad (4.7)$$

where  $U^n$  is the column matrix with  $u_k^n$  as elements. Matrices  $A^n$  and  $B^n$  are tridiagonal with the following elements:

$$A_{k,k}^n = -\frac{i}{h^2} + \frac{i}{2} f_k^n \quad A_{k+1,k}^n = A_{k,k+1}^n = \frac{i}{2h^2} \quad k=1,2,\dots,K \quad (4.8)$$

$$A_{k,j}^n = 0 \quad \text{for } k \neq j \quad k \neq j+1$$

$$B_{k,k}^n = 1 - i\tau\sigma \left( \frac{1}{h^2} - \frac{f_k^n}{2} \right) \quad B_{k+1,k}^n = B_{k,k+1}^n = \frac{i\tau\sigma}{2h^2} \quad k=1,2,\dots,K \quad (4.9)$$

$$B_{k,j}^n = 0 \quad \text{for } k \neq j \quad k \neq j+1$$

The solution of the matrix equation (4.7) is

$$U^{n+1} = U^n - (B^n)^{-1} \tau (A^n U^n) \quad (4.10)$$

To get the second term on the right-hand side of (4.10),  $A^n$  is first multiplied by  $U^n$ , already known from the previous step, and then the matrix equation  $B^n X = A^n U^n$  is solved. Because  $B^n$  is tridiagonal, the matrix inversion can be

avoided by using the Gaussian elimination. The so-called Thomas algorithm is most often used. The system of equations is written in the form

$$a_k x_{k-1} + c_k x_k + b_k x_{k+1} = d_k \quad k = 2, 3, \dots, K-1$$

$$c_1 x_1 = -b_1 x_2 + d_1 \quad (4.11)$$

$$c_K x_K = -a_K x_{K-1} + d_K$$

The solution is assumed to be in the form

$$x_k = \alpha_{k+1} x_{k+1} + \beta_{k+1} \quad (4.12)$$

where

$$\alpha_2 = -c_1/c_1 \quad \beta_2 = x_1/c_1$$

$$\alpha_{k+1} = \beta_k / (a_k \alpha_k + c_k) \quad (4.13)$$

$$\beta_{k+1} = (d_k - a_k \beta_k) / (a_k d_k + c_k)$$

Noting that  $x_K = \beta_{K+1}$  the unknowns  $x_k$  are successively found from (4.12). It has been shown that this scheme does not introduce large errors due to round-off errors in the calculations (Ames, 1969) and is very efficient in terms of computer time.

A complete program for solving the parabolic equation is given in the Appendix.

## 5. NUMERICAL RESULTS AND DISCUSSION

The parabolic equation (3.1) has been solved for a model equatorial plasma bubble filled with irregularities whose horizontal structure is the same as the one measured in-situ by McClure et al. (1977) and shown in their Figure 7. The satellite altitude was approximately 280 km and probably did not change appreciably during the passage through a bubble whose horizontal size was  $\sim 50$  km. The F-peak height at the time of the measurements was approximately 400 km.

After enlargement, the curve in Figure 7 of McClure et al. was digitized every 42 m which is approximately 10 m less than the sampling interval of in-situ measurements. This sets the lower limit on the irregularity scale-size or the scale length of the electron density gradient. It is still much less than the Fresnel zone dimension for a typical distance between the bottom-side of the irregular layer and the receiver (200-300 km) and the highest wave frequency considered in this report, which is 6 GHz.

To have some impression about the irregularity spectrum, the digitized data were high-pass filtered to remove any components larger than 10 km and the power spectrum was computed. Figure 5 shows that the spectral amplitude roughly follows the  $\kappa^{-1}$  law except for the extreme point at the low frequency part of the spectrum. This is a very typical spectrum of ionospheric F region irregularities (Dyson et al., 1974).

We assumed that the relative electron density fluctuations at each height inside a bubble follow the same horizontal pattern as one given in Figure 1. The background density is parabolic as described in Section 2. With the weighting function corresponding to the "initial stage" of a bubble, before it rose above the F-peak, the horizontal absolute electron density variation  $\Delta N$  at four different levels inside the bubble is given in Figure 4a. The largest  $\Delta N = 1.7 \cdot 10^5 \text{ electrons} \cdot \text{cm}^{-3}$  is reached close to the center of the bubble. If the bubble thickness  $L$  is defined as a distance between levels at which the weighting function falls to  $e^{-1}$ , we have  $L=30 \text{ km}$ .

The second extreme case to be discussed corresponds to the "developed stage" of a bubble (Figure 4b). In this case, the maximum  $\Delta N$  is approximately equal to  $2 \cdot 10^5 \text{ electrons} \cdot \text{cm}^{-3}$  and the bubble thickness  $L=115 \text{ km}$ .

The scintillation pattern resulting from our computations for a wave of frequency 1.5 GHz passing through the initial stage bubble is shown in Figure 6. The real and imaginary components of the complex amplitude as well as amplitude and phase in  $\pi$  units are depicted. The most interesting feature is the correspondence between the position of strong amplitude outbursts and the location of sharp electron density gradients in Figure 1. This seems to suggest the refractive scattering mechanism proposed by Crain et al. (1979) as a cause of appreciable scintillation. However, as we show later in this section the diffraction on edges

more easily explains the obtained feature. It is also interesting to note one more striking peculiarity, namely, the weak dependence of the amplitude outbursts on the absolute value of electron density deviation  $\Delta N$ .

For a developed, thick bubble the edge effect is largely obscured by amplitude fluctuations attributed to scattering or diffraction by smoother structure (Figure 7). Nevertheless, stronger amplitude scintillation can still be noted close to sharp gradients of  $\Delta N$ . On lower frequencies the edge effect can hardly be distinguished from scattering (Figure 8b). However, its presence can be seen from Figure 8a, which shows the amplitude pattern at 300 km height, i.e., inside the bubble. Evidently, the edge diffraction develops amplitude fluctuations at shorter distances than does the scattering.

To discuss further the effect of an isolated sharp gradient in electron density, we assumed a wave passing through a one-dimensional screen which at the point  $x=x_0$  changes the wave's phase from 0 to some constant value  $\phi_0$ . The complex amplitude at a distance  $z$  is given by

$$u(x, z) = \sqrt{\frac{k}{2\pi iz}} \int_{-\infty}^{\infty} u(x', 0) \exp[ik \frac{(x-x')^2}{2z}] dx', \quad (5.1)$$

where

$$\begin{aligned} u(x, 0) &= e^{i\phi_0} \text{ for } x > x_0 \\ &= 1 \text{ for } x < x_0 \end{aligned} \quad (5.2)$$

Simple integration and separation of the real and imaginary parts of  $u(x, z)$  lead to the following formulae

$$\begin{aligned} \operatorname{Re} u(x, z) = & \cos^2 \frac{\phi_0}{2} - \frac{1}{2} \{ [1 - \sqrt{2} \cos (\frac{\pi}{4} - \phi_0)] C(\alpha) \\ & + [1 - \sqrt{2} \sin (\frac{\pi}{4} - \phi_0)] S(\alpha) \}, \end{aligned} \quad (5.3)$$

$$\begin{aligned} \operatorname{Im} u(x, z) = & \frac{1}{2} \sin \phi_0 - \frac{1}{2} \{ [1 - \sqrt{2} \cos (\frac{\pi}{4} - \phi_0)] S(\alpha) \\ & - [1 - \sqrt{2} \sin (\frac{\pi}{4} - \phi_0)] C(\alpha) \}, \end{aligned} \quad (5.4)$$

where  $S(\alpha)$  and  $C(\alpha)$  are the Fresnel integrals of the argument  $\alpha = (x - x_0) \sqrt{k/2z}$ . Equations (5.3) and (5.4) were used to obtain the diffraction pattern at a distance  $z = 350$  km from a screen for frequencies of 360 MHz and 4 GHz with  $\phi_0 = 16.4$  and 1.48, respectively. The sudden phase jump was put at  $x = 3$  km. Results of the calculations are shown in Figure 9. A typical oscillatory pattern can be noticed. Oscillations are much faster at 4 GHz and damped at shorter distances from the discontinuity, therefore, the edge effect is more localized in this case than at lower frequency. This explains why at higher frequencies it is easier to find the correspondence between sharp electron density gradients and the characteristic wave amplitude pattern. At lower frequencies the effect of closely spaced sharp gradients leads to a rather complicated picture not resembling the pattern produced by localized discontinuities. Thus, the edge effect is not seen in Figure 8b.

Crain et al. (1979) suggested the refractive scattering mechanism as a possible cause of scintillation at gigahertz frequencies. This mechanism involves a total internal

reflection from vertically extended horizontal discontinuities of electron density. Under some strict conditions imposed on the slope of discontinuity, the direct wave interferes with the unattenuated, reflected wave leading to strong amplitude fluctuations. A thorough discussion of the mechanism would require ray tracing in the model bubble with sharp boundaries. However, if the maximum grazing angle is small the parabolic equation offers an adequate mathematical description of the effect. Thus, we might expect that our calculations take into account refractive scattering. To check the importance of refractive scattering relative to the diffraction on edges, we computed the diffraction pattern produced by a screen which changes the phase of the wave proportionally to  $\Delta N$  given by in-situ data. The proportionality constant was chosen such as to achieve the best agreement between the phase variations at a distance of 350 km from a screen with those at a distance 400 km from the top of a bubble when the full model is used. We wish to note at this point that the phase screen was placed not in the middle of the scattering layer (approximately 300 km height) but above the layer (cf. Figure 3a). This was necessary in order to make allowance for the development of amplitude scintillation as strong as that given by the solution of the parabolic equation. This remark might be of some importance to those who use the strong phase screen theory in interpreting the data.

Figures 10 and 11 present the comparison of the amplitude and phase variations at 360 and 4000 MHz as produced

by the phase screen and the initial stage model bubble. Close inspection of the figures indicates a remarkable similiarity between amplitude and phase structures with only slightly deeper fading at 360 MHz produced by the bubble. We conclude that at least to the order of approximation given by the parabolic equation the refractive scattering is either of no importance as compared to the edge diffraction effect or both effects are indistinguishable.

In Figures 12 and 13 we present the amplitude fluctuations at several frequencies for the initial and developed stages of the bubble, respectively. The edge effect is clearly seen on gigahertz frequencies in the developed stage and even at 800 MHz in the case of the initial bubble stage. It is interesting to note an increase in the fading rate as the bubble thickens. This is clearly seen at all frequencies except at 4 GHz which is dominated by the edge effect. This agrees very well with measurements (Basu et al., 1977) showing rising amplitude fading rate when the bubble develops and extends above the F-peak. At the outskirts of the bubble (distance larger than 15 km), scintillation intensity and fading rate are smaller than those closer to the center, mainly due to the deficiency of small scale electron density irregularities. The fading rate, which is also changing with frequency, is usually larger at lower frequencies. This is in agreement with observations by Rino et al., (1978) but contrary to the weak scatter

30

scintillation theory which predicts the dominant fading period proportional to the Fresnel zone size  $\sqrt{\lambda z}$ . However, when scintillation is strong, as in our case at frequencies below 4 GHz, the multiple scattering effects reduce the characteristic size of the wave field fluctuations leading to the increase of the fading rate (Yeh et al., 1975). The practical importance of the scintillation index justifies its calculations in spite of the obvious nonstationarity of the computed amplitude pattern noticeable especially at higher frequencies. The  $S_4$  scintillation index was calculated only for the segment of data from  $x=0$  to 15 km. The segment of  $x=15$  to 25 km shows clearly a different amplitude structure due to the lack of small-scale electron density irregularities. Between  $x=0$  and 15 km, scintillation indices calculated for each 5 km data segment differed not more than 25% which gives the impression about the stationarity assumption. The frequency dependence of scintillation index is shown in Figure 14. For moderately strong scintillation ( $S_4 < 0.5$ ),  $S_4$  is proportional to  $f^{-\nu}$  with  $\nu$  between 1 and 1.5. However, the index  $\nu$  is closer to 1.5 for the scintillation index smaller than 0.2. As one would expect, the stronger the scintillation the weaker is its frequency dependence. We must point out, however, that at low frequencies the assumptions leading to the parabolic equation might break down. In fact, at 136 MHz in the case of a thick, developed bubble, the average intensity is about 15% lower than the intensity of the incident wave. This means that 15% of the

incident power is backscattered from the irregular layer, which no longer is small. In other cases under consideration, the backscattered power was less than 10% of the incident power. Figure 15 shows the case when the average signal level close to the center of the bubble is much below the level of the incident wave. In this particular example, only about 77% of the power is transmitted through the bubble. The result shown in Figure 15 was for frequency wave of 136 MHz passing through the extended bubble and the F-peak electron density was  $3.5 \cdot 10^5$  electrons  $\cdot \text{cm}^{-3}$ . It would be interesting to examine the observational data to find cases where strong scintillation is accompanied by a decrease in the signal level. If such cases could be found, this would indicate the need for modification of the scintillation theory based on the parabolic equation.

It is interesting to compare the scintillation pattern produced by a bubble with sharp electron density gradients to that given by a bubble with random irregularities. To do that the electron density profile shown in Figure 1 was low-pass filtered with the cut-off wave number  $0.1 \text{ km}^{-1}$ . The high-frequency component of the data was obtained by subtracting low-frequency part from the original data. The high-frequency component of the data was then Fourier analyzed and the amplitude and phase of each Fourier component was determined. Following the procedure used by Costa and Kelley (1978) a random phase angle was added to

each phase, the data were then transformed back to the spatial domain and added to the low-frequency component of the original data. As a result we obtained the electron density profile with random high-frequency component which has the same power spectrum and variance of the electron density as the high-frequency component of the original data. Two examples of such profile generated using different random numbers are shown in Figures 16a and 16b. Note that sharp spikes and gradients clearly seen in Figure 1 are not present on these profiles. On the other hand, they contain more weak, small-scale structures.

The scintillation pattern produced by the "initial stage" bubble with horizontal electron density profiles as shown in Figures 16 was calculated leading to the result shown in Figure 17. At 4 GHz almost no scintillation is seen. The weakness of scintillation is confirmed by the calculated scintillation index of 0.02 for both runs. This is approximately half of the scintillation index calculated when the original profile is used. The variance of the high-frequency electron density component is equal to  $6.6 \cdot 10^3$  electrons $\cdot$ cm $^{-3}$  which is only slightly smaller than that for the original data ( $7.7 \cdot 10^3$  electrons $\cdot$ cm $^{-3}$ ). Thus the two-fold decrease in the scintillation index can not be explained by the difference in  $\langle (\Delta N)^2 \rangle$  since in the weak scattering scintillation theory the scintillation index  $S_4$  is directly proportional to  $\langle (\Delta N)^2 \rangle^{1/2}$ . Therefore, random electron density fluctuations would have to be stronger (in our case two times stronger) to give scintillation as strong as that

produced by a medium dominated by sharp electron density gradients. Also at lower wave frequencies the scintillation index is enhanced by the presence of sharp electron density gradients. For instance, at 360 MHz for the original electron density profile  $S_4=0.64$  while the randomized profiles lead to  $S_4=0.45$  and  $0.52$ , for run A and B, respectively. Obviously, the difference between the scintillation indices is smaller than at higher frequencies because of the effect of strong scattering which reduces the scintillation index dependence on  $\langle \Delta N^2 \rangle$ .

Sometimes observational data are represented in the form of scatter plots on the plane Imu-Reu. For completeness, we show in Figure 18 several such plots, all of them obtained using the same "initial stage" bubble model and differing in the wave frequency only. No filtering to separate the focus and scatter components was applied mainly because of the nonstationarity of the imaginary and real parts of the complex amplitude and difficulty in choosing the appropriate cut-off wave number. Nevertheless, it is interesting to note the obvious similarity between the model plots and plots derived from the scintillation data (cf. Fremouw et al., 1978). Both the model and data show a clear change from the phase dominated scintillation at high frequencies to the dominance of the scatter component with the power evenly distributed between Imu and Reu at lower frequencies.

In our model we have assumed that the relative electron density fluctuation  $\Delta N/N$  does not depend on the height inside

a bubble. This assumption leads to the exaggerated phase fluctuations and possibly also to the overestimated scattering effects in amplitude. However, the edge diffraction effect is correctly predicted.

## 6. CONCLUSIONS

Solution of the parabolic equation for the complex amplitude of a wave passing through a simple model of an equatorial bubble revealed the importance of sharp horizontal gradients of the electron density in producing scintillation effects. Preliminary discussion of the effects suggests the diffraction on edges formed by sharp gradients as a possible mechanism of scintillation. The edge effect is particularly important at higher gigahertz frequencies where it is not obscured by scattering. The important fact is that the edge diffraction leads to appreciable scintillation even if  $\Delta N$  is quite moderate and  $L$  is small.

The computed amplitude scintillation pattern is in good agreement with the observations, which indicate an increase of the scintillation rate with the increase of the bubble thickness and show a change in the scintillation rate from slow, close to the edges of the bubble, to fast, at its center. The frequency dependence of scintillation is of the type  $f^{-\nu}$  with  $\nu$  between 1 and 1.5 at gigahertz frequencies. There is a tendency toward smaller values of  $\nu$  as the bubble thickens.

The bubble model we have used is deterministic. Due to the obvious nonhomogeneity of electron density fluctuations, it is difficult to compare the obtained results with those based on the statistical scintillation theory. Nevertheless, we have shown that the model of random irregularities

characterized by the same power spectrum as the medium with sharp electron density gradients produces less scintillation not only at GHz frequencies but also at lower frequencies where the scattering effects should be dominating. Apparently, the increased strength of scintillation can be attributed to the diffraction on sharp edges--the scintillation mechanism which is not taken into account by the statistical scintillation theory.

## REFERENCES

- Ames, W. F., Numerical Methods for Partial Differential Equations, Barnes & Noble, Inc., New York, 1969.
- Basu, S., J. Aarons, J. P. McClure, C. LaHoz, A. Bushby, and R. F. Woodman, "Preliminary Comparisons of VHF Radar Maps of F-region Irregularities with Scintillations in the Equatorial Region", J. Atmos. Terr. Phys., v.39, pp.1251-1261, 1977.
- Basu, S., and M. C. Kelley, "Review of Equatorial Scintillation Phenomena in Light of Recent Developments in the Theory and Measurements of Equatorial Irregularities," J. Atmos. Terr. Phys., v.39, pp.1229-1242, 1977.
- Basu, S., and M. C. Kelley, "A Review of Recent Observations of Equatorial Scintillations and Their Relationships to Current Theories of F-region Irregularity Generation," Radio Sci., (in press, 1979).
- Basu, S., S. Basu, J. Aarons, J. P. McClure and M. D. Cousius, "On the Coexistence of Kilometer-and Meter-Scale Irregularities in the Night-time Equatorial F Region," J. Geophys. Res., v.83, No.A9, pp.4219-4226, 1978.
- Borodziewicz, W., "Approximate Solution of the Equation for the Second Moment of the Wave Function," (Unpublished manuscript) Space Research Center, Polish Academy of Sciences, Warsaw, Poland, 1978.
- Costa, E., and M. C. Kelley, "On the Role of Steepened Structures and Drift Waves in Equatorial Spread F." v.83, J. Geophys. Res., v.83, No.A9, pp.4359-4364, 1978.

- Crandall, S. H., "An Optimum Implicit Recurrence Formula for the Heat Conduction Equation," *Quart. App. Math.*, v.13, pp.318-320, 1955.
- Crain, C. M., H. G. Booker, and J. A. Ferguson, "Use of Refractive Scattering to Explain SHF Scintillation", *Radio Sci.*, v.14, pp.125-134, 1979.
- Dyson, P. L., J. P. McClure, and W. B. Hanson, "In situ Measurements of the Spectral Characteristics of F Region Ionospheric Irregularities", *J. Geophys. Res.*, v.79, pp.1497-1502, 1974.
- Farley, D. T., B. B. Balsley, R. F. Woodman, and J. P. McClure, "Equatorial Spread F: Implications of VHF radar observations," *J. Geophys. Res.*, v.75, 7199, 1970.
- Haerendel, G., "Theory of equatorial spread-F", Preprint, Max-Planck-Institut für Physik und Astrophysik, Garching, W. Germany, 1974.
- Kelley, M. C., and E. Ott, "Two-Dimensional Turbulence in Equatorial Spread F," *J. Geophys. Res.*, v.83, pp.4369-4372, 1978.
- Koster, J. R., "Study of the Equatorial Ionosphere," Report AFGL-TR-77-0165, University of Ghana, Legon, Ghana, 1976.
- McClure, J. P., W. B. Hanson and J. H. Hoffman, Plasma bubbles and irregularities in the equatorial ionosphere, *J. Geophys. Res.*, v.82, 2650-2656, 1977.
- Ossakow, S. L., S. T. Zalesak and B. E. McDonald, and P. K. Chaturvedi, "Nonlinear Equatorial Spread F: Dependence on the Altitude of the F Peak and Bottomside Background Electron Density Gradient Scale Length," *J. Geophys. Res.*, v.84, pp.17-23, 1979.

- Ott, E., "Theory of Rayleigh-Taylor Bubbles in the Equatorial Ionosphere," J. Geophys. Res., v.83, pp.2066-2070, 1978.
- Scanapieco, A. J., and S. L. Ossakow, "Nonlinear Equatorial Spread F," Geophys. Res. Letts., v.3, p.451, 1976.
- Skinner, N. J., R. F. Kelleher, J. B. Hacking, and C. W. Benson, "Scintillation Fading of Signals in the SHF Band", Nature, v.232, p.19, 1971.
- Rino, C. L., R. A. Long, M. D. Cousins, and R. C. Livingston, "Continued Performance of the Wideband Satellite Experiment", Bimonthly Progress Report #5, SRI International Project 6436, SRI International, Menlo Park, CA. 94025, 1978.
- Tatarski, V. I., "The Effects of the Turbulent Atmosphere on Wave Propagation", U.S. Department of Commerce, National Technical Information Service, Springfield, Va., 1971.
- Taur, R. R., "Simultaneous 1.5 and 4 GHz Ionospheric Scintillation Measurements", Radio Sci., v.11, pp.1029, 1976.
- Weber, E. J., J. Buchau, R. H. Eather, and S. B. Mende, "North/South Aligned Equatorial Airglow Depletions," J. Geophys. Res., v.83, pp.712-716, 1978.
- Woodman, R. F., and C. LaHoz, "Radar Observations of F Region Equatorial Irregularities," J. Geophys. Res., v.81, p.5447, 1976.
- Yeh, K. C., C. H. Liu and M. Y. Youakim, "A Theoretical Study of the Ionospheric Scintillation Behavior Caused by Multiple Scattering", Radio Sci., v.10, pp.97-106, 1975.
- Yeh, K. C., H. Soicher, and C. H. Liu, "Observations of Equatorial Ionospheric Bubbles by the Radio Propagation Method," J. Geophys. Res. (in press, 1979).

## APPENDIX

In this appendix the algorithm and computer program (in CDC FORTRAN Extended) used to solve the two-dimensional parabolic equation (4.1) are given. The employed method is described in Section 4.

The program was made versatile to be used with an arbitrary model of the irregular ionosphere, but also to make possible calculations for a wave which propagates in a free space after traversing an irregular layer or a wave disturbed by a phase changing screen.

The input parameters are:

- K - number of steps in the horizontal x direction,
- N - number of steps in the vertical z direction,
- TAU - step-size in the z direction (in m),
- H - step-size in the x direction (in m),
- SIGM - weighting factor (our choice was SIGM=0.51),
- FREQ - wave frequency (in MHz),
- N1 - N1=1 for the phase screen model,
- KSKIP - number of steps in the z direction recorded on the file PASS (which is the renamed file RESULT) over which one has to skip to get to the z level from which further computations will be made. This is used whenever one wants to continue computations with the changed step-size TAU, or when further computations are to be made outside a scattering medium.
- XM - only every XM step in the z direction is recorded on files RESULT and TERM
- KK - only every KK step in the x direction is recorded on file TERM.

- IC - used as an indicator. If IC=1 computations are made inside the scattering medium, if IC=0, for computations outside a medium and for the phase screen model.
- KL - total number of steps in the z direction calculated in the previous runs. KL is used to calculate the overall distance passed by a wave.
- NP - used as the reading indicator. If NP>0 input parameters recorded on the file PASS are read. Otherwise it is assumed that they were not recorded.
- K2 - K2=0 if the input file ELFL must be read. It does not need to be read for computations outside a scattering medium, but must be read at the beginning of the phase screen computations.
- PHLØ - phase variance or a constant converting data stored on ELFL to phase variations.

The above parameters are universal and must be supplied whenever the program is used. Below, the described parameters which apply only to the model of a plasma bubble discussed in the report:

- AL and ZO - weighting function at the top of a bubble is changing according to  $\text{EXP}(-((Z-ZO)/AL)**2)$
- BET and ZOO - weighting function at the bottom of a bubble is changing according to  $\text{EXP}(-((Z-ZOO)/BET)**2)$ . For Z.GE.ZO and Z.LE.ZOO the weighting function is constant and equal 1.
- ZMAX - height of the F-peak measured
- ELMAX - electron density at the F-peak in  $\text{electrons}\cdot\text{cm}^{-3}$
- ELZ - electron density at Z=0 in  $\text{electrons}\cdot\text{cm}^{-3}$ .

Note that Z=0 corresponds to a height at which computations start. All distances are in meters.

All input parameters are read from the file DA2. Horizontal variations in a medium or on a phase screen are given

in arbitrary units and read from the file ELFL. Results of computations are written on the files RESULT and TERM. RESULT contains high-accuracy results intended to be used for plotting or further calculations. In the later case this file must be renamed to PASS and will be read during the next program run. TERM is used only for printing purposes and has the same content as RESULT.

Instead of using the COMPLEX variables the program uses the matrix representation of complex variables with the first column being the real part and the second column the imaginary part of a variable.

Subroutine YO sets the initial values to the matrix representing the complex amplitude. If the phase screen model is used, subroutine YOI sets values of the complex amplitude on the screen. If KSKIP.NE.O initial values are read from PASS.

Using the model of irregularities, subroutine FLUCT calculates dielectric permittivity fluctuation and its mean value at two adjacent  $z$  levels.

Both  $A$  and  $B$  matrices of equation (4.7) are stored in the form of three matrices:  $A$ ,  $B$ , and  $C$ , and  $AA$ ,  $BB$  and  $CC$ . Matrices  $A$  and  $B$  contain off-diagonal elements of the matrix  $A$ , and matrix  $C$  contains diagonal elements of  $A$ . Note that  $A=B$ . Similarly,  $AA$  and  $BB$  contain off-diagonal elements of the matrix  $B$ , while in  $CC$  its diagonal elements are stored. Again  $AA=BB$ . The program was written assuming

that  $A=B$  and  $AA=BB$  but it should not be any problem with its generalization.

Elements of the matrix  $C$  are calculated in the subroutine CTAB using output from the subroutine FLUCT. If the model assumes no changes of the electron density in the  $z$  direction, matrices  $C$  and  $CC$  can be calculated outside the loop

```
DO 2 J=1,N.
```

Subroutine MOZAX performs the matrix multiplication. It multiplies the matrix  $A$  by the matrix  $Y$  which contains the complex amplitude at the preceding level or the initial values.

Subroutine PROGON solves the system of equations using the Thomas algorithm described in Section 4.

```

*****
THE MODEL OF THE REGULARITIES IS CALCULATED IN THE SUBROUTINE FLUCT SUB-
ROUTINE VO IS USED TO SET THE INITIAL VALUES FOR A PHASE SCREEN THEY
ARE CALCULATED IN THE SUBROUTINE VOI SUBROUTINE CTAB CALCULATES ELE-
MENTS OF THE MATRIX C, SUBROUTINE HOPAR IS USED TO CALCULATE THE PRO-
DUCT OF TWO MATRICES, AND THE SUBROUTINE PROCON TO SOLVE THE SYSTEM
*****

```

[illegible]

```

INPUT PARAMETER
N=NUMBER OF STEPS IN THE HORIZONTAL X DIRECTION
M=NUMBER OF STEPS IN THE VERTICAL Z DIRECTION
NU=STEP SIZE IN THE X DIRECTION IN M
MV=STEP SIZE IN THE Z DIRECTION IN M
PAG=THE WEIGHTING FACTOR (DENominator)
PAG=NU*MV ON THE PHASE SCREEN
NAP=NUMBER OF STEPS IN THE X DIRECTION RECORDED ON THE FILE PASS
(RENAMED FILE RESULT) OVER WHICH ONE HAVE TO BRIP TO FIND THE INITIAL
VALUES FOR FURTHER COMPUTATIONS IF THEY WERE STOPED FOR ANY
REASON (FOR INSTANCE, TRANSITION FROM COMPUTATIONS INSIDE THE MEDIUM
TO THOSE OUTSIDE THE MEDIUM)
RM=ONLY EVERY RM STEP IN THE X DIRECTION IS RECORDED ON FILES RESULT
AND TERM
RR=ONLY EVERY RR STEP IN THE Z DIRECTION IS RECORDED ON THE FILE TERM
IC=1 FOR COMPUTATIONS INSIDE THE IRREGULAR MEDIUM, IC=0 OUTSIDE
THE MEDIUM AND FOR THE PHASE SCREEN
RL=NUMBER OF STEPS IN THE X DIRECTION COMPUTED IN THE PREVIOUS RUNS
(USED TO CALCULATE A DISTANCE FROM Z=0 TO THE ACTUAL LEVEL)
UP=1 IF USER PASS A READING INDICATION, IF NPO=1 INPUT VALUES RECORDED ON
THE FILE PASS ARE READ, OTHERWISE IT IS ASSUMED THAT THEY WERE NOT
RECORDED
K2= IF K2=0 THE INPUT FILE EPL IS READ, IT DOES NOT NEED TO BE READ
FOR CALCULATION OUTSIDE THE IRREGULAR MEDIUM
REMARK: THE REST OF PARAMETERS APPLY ONLY TO THE IRREGULARITY MODEL
DESCRIBED IN THE REPORT
PHASE=1, 2, 3 ARE USED TO CALCULATE THE WEIGHTING FUNCTION
PHASE=0 ARE USED TO CALCULATE THE PARABOLIC ELECTRON CONCENTRATION
PROFILE, PHASE IS THE ASSUMED RMS PHASE ON THE PHASE SCREEN

```







[illegible]



[illegible]



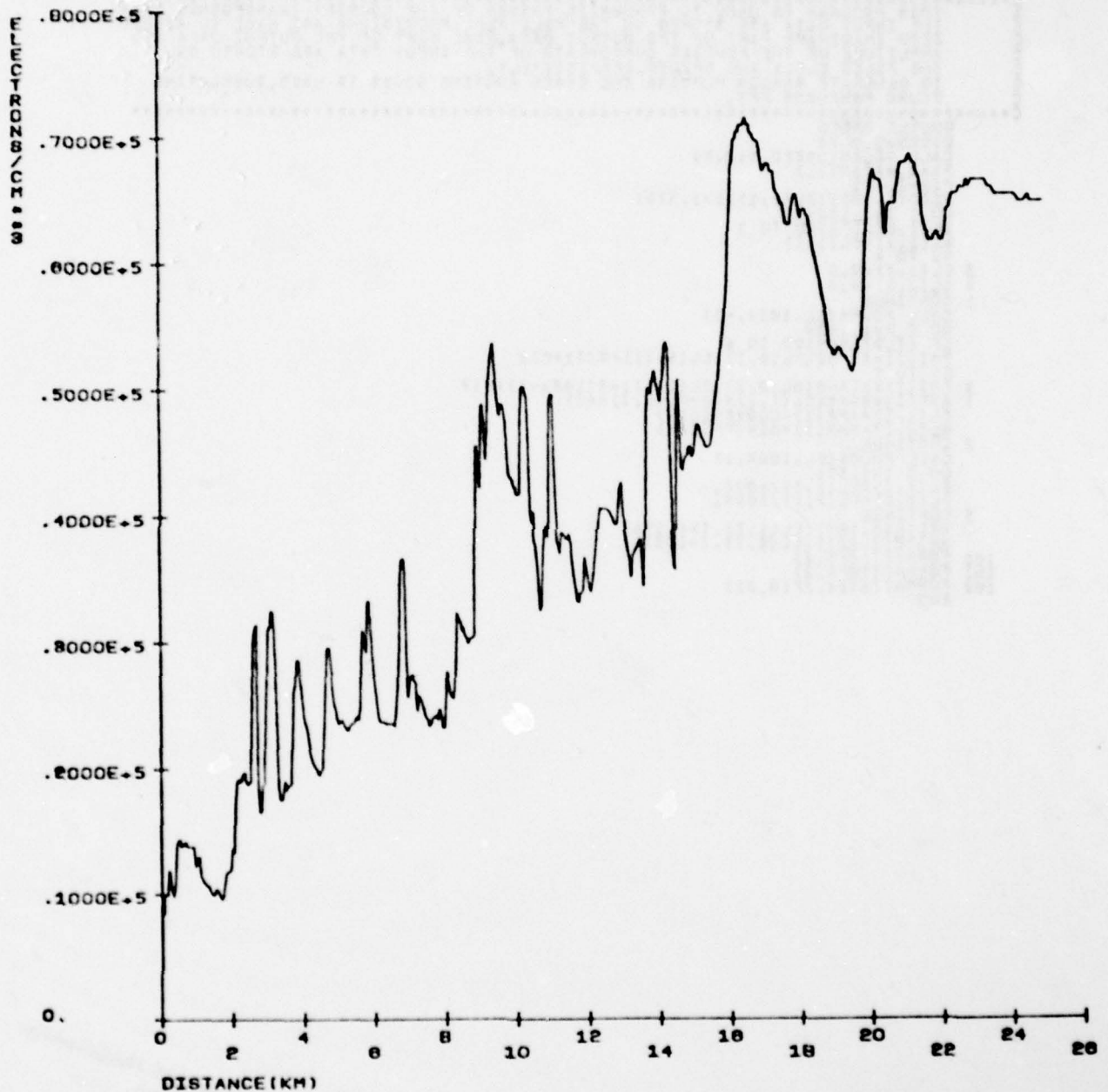


Fig. 1. High resolution electron density profile measured inside the plasma bubble. (Figure 7 of McClure et al. (1977) reconstructed after digitization.)

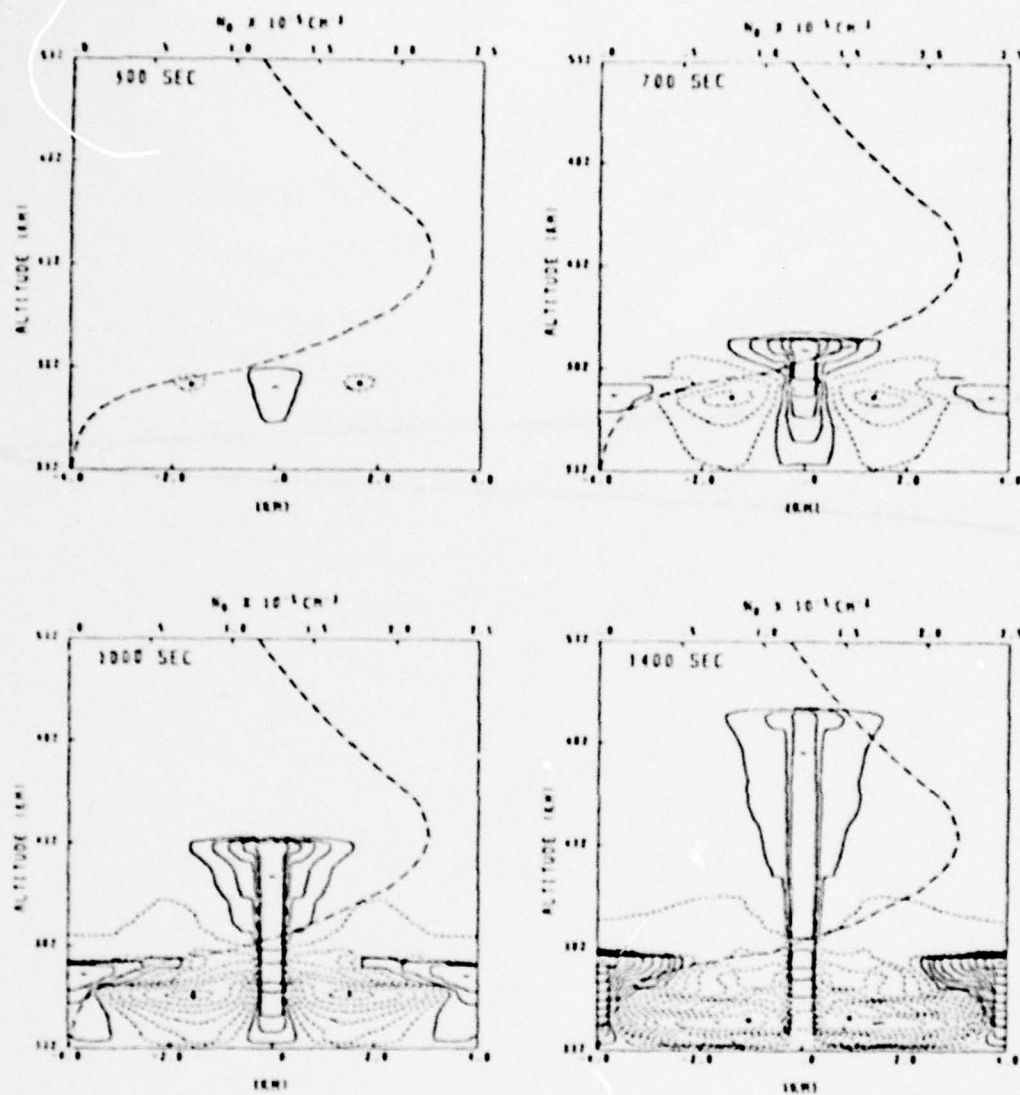


Fig. 2. Contour plots of constant  $\Delta N/N$  at different stages of the bubble evolution as given by numerical simulation (Ossakow et al., 1979).

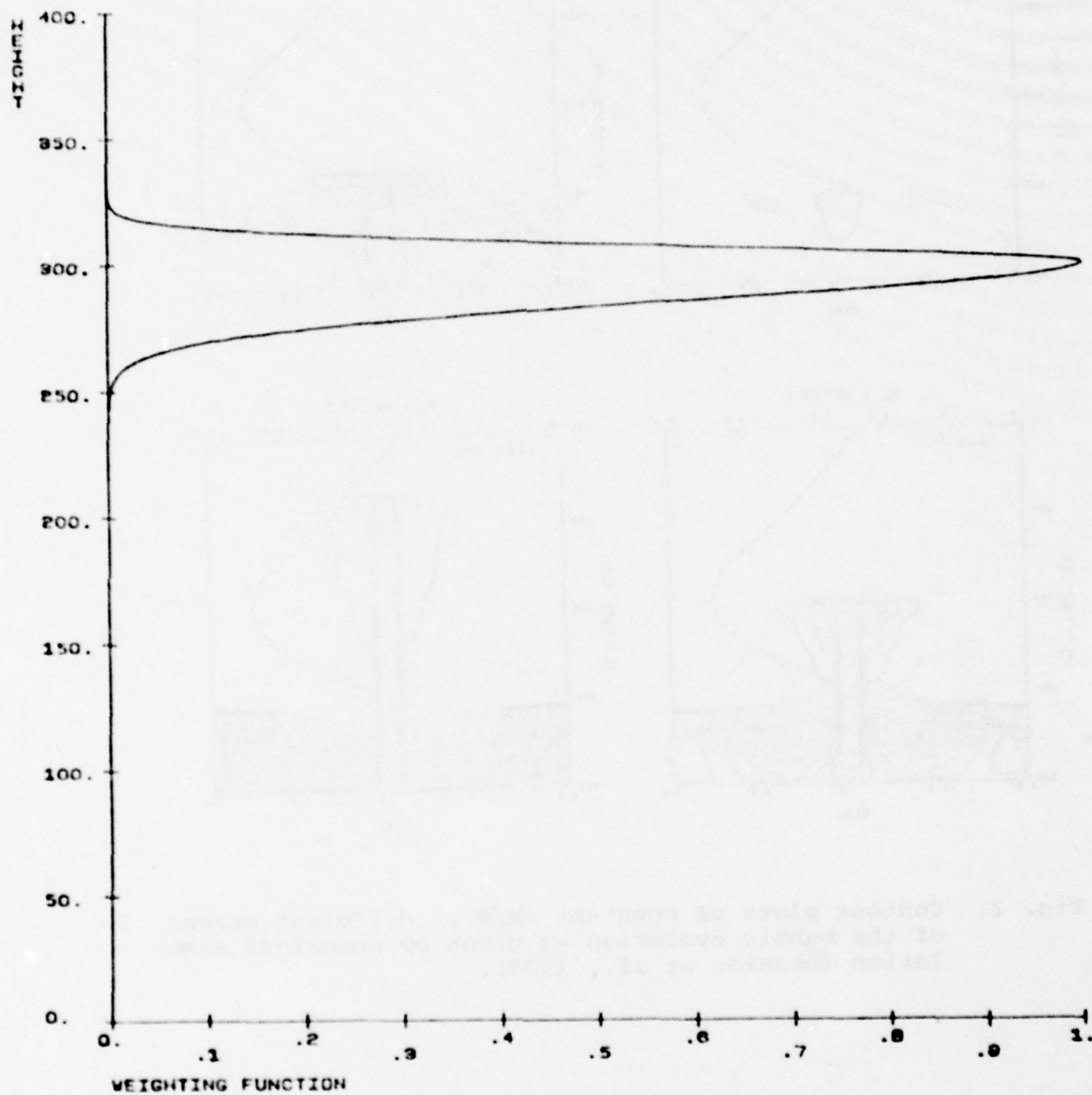


Fig. 3A. Weighting functions used to model "initial stage" of plasma bubble.

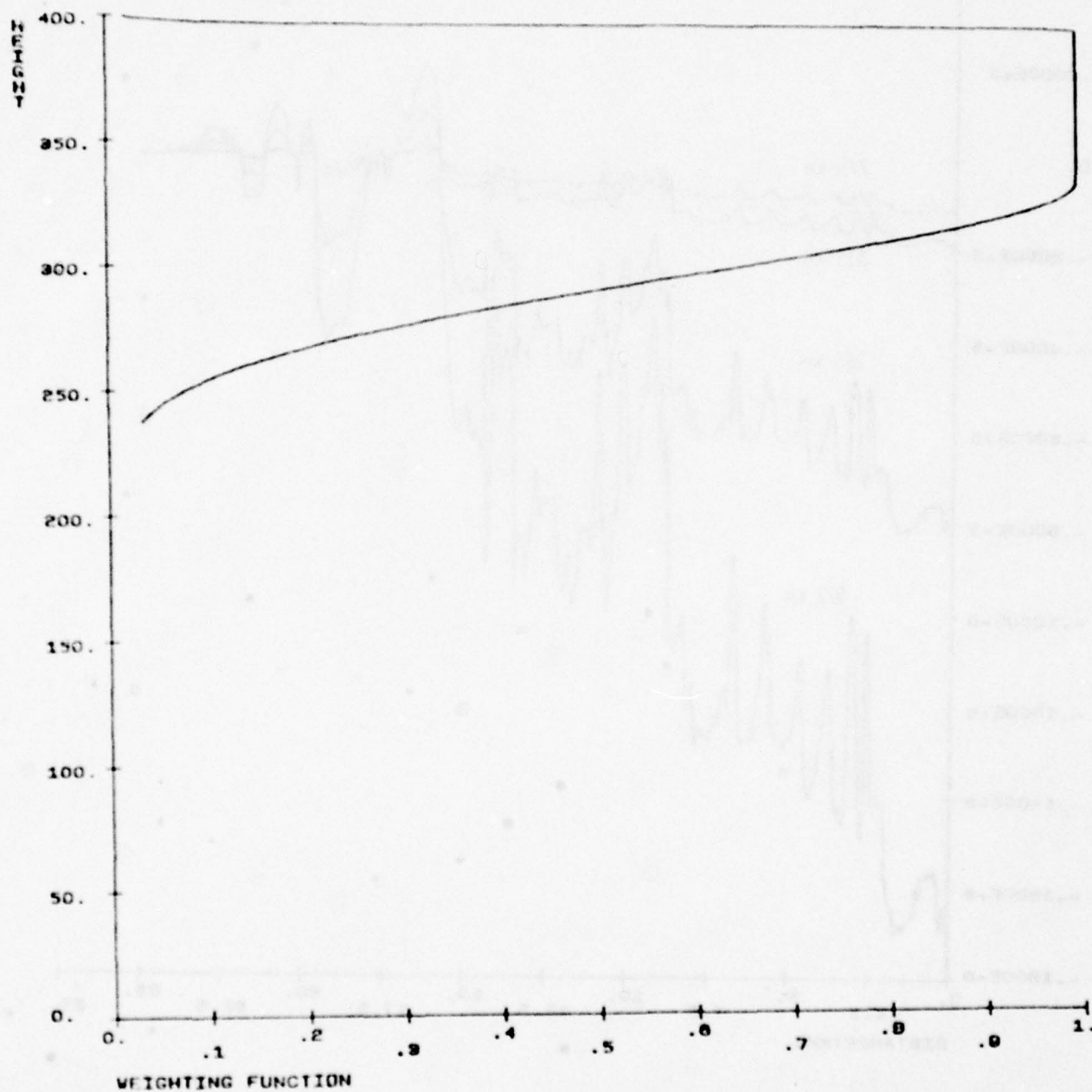


Fig. 3B. Weighting functions used to model "developed stage" of plasma bubble.

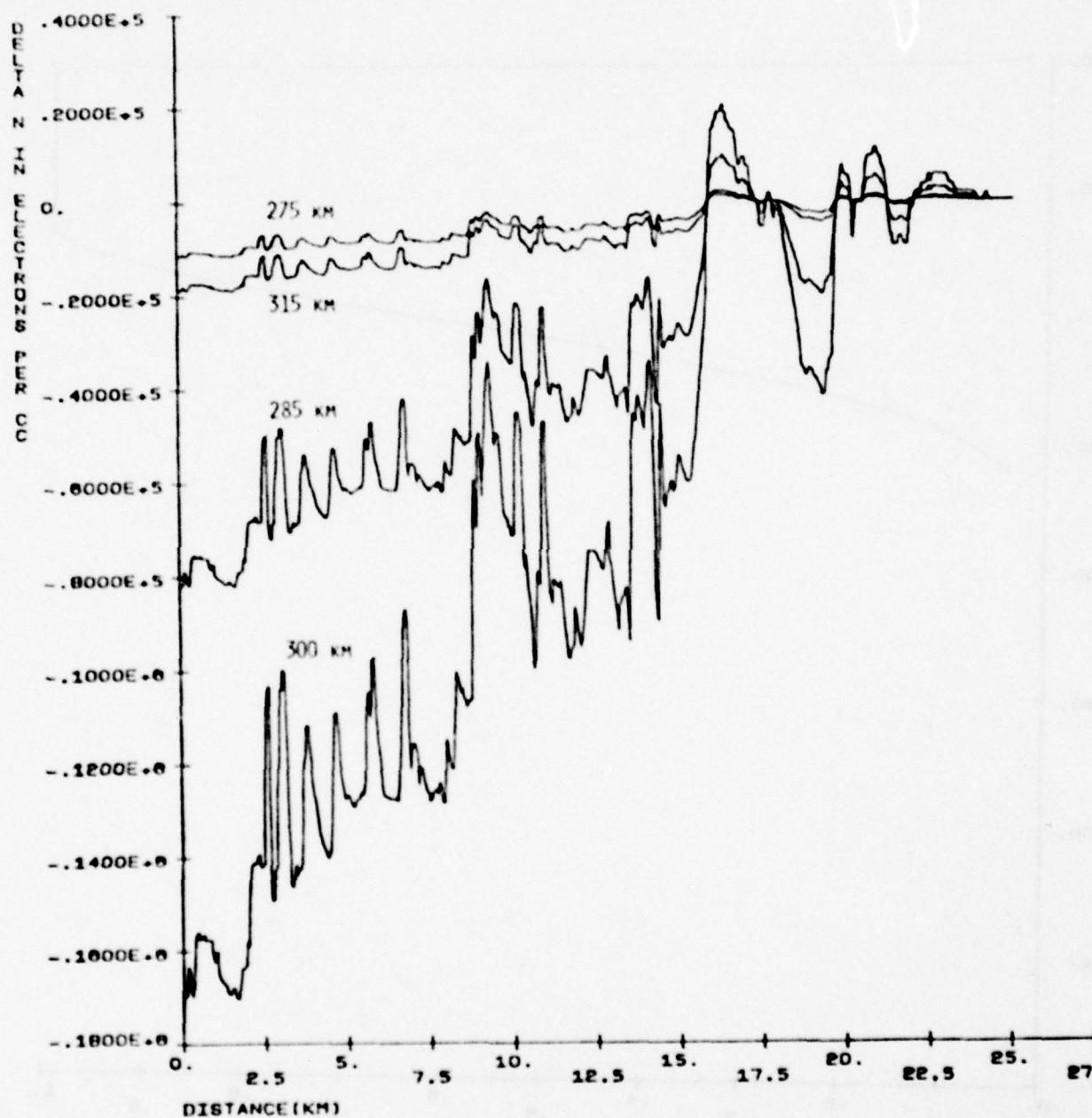


Fig. 4A. Horizontal electron density fluctuation profiles at different heights inside a plasma bubble, "initial stage."

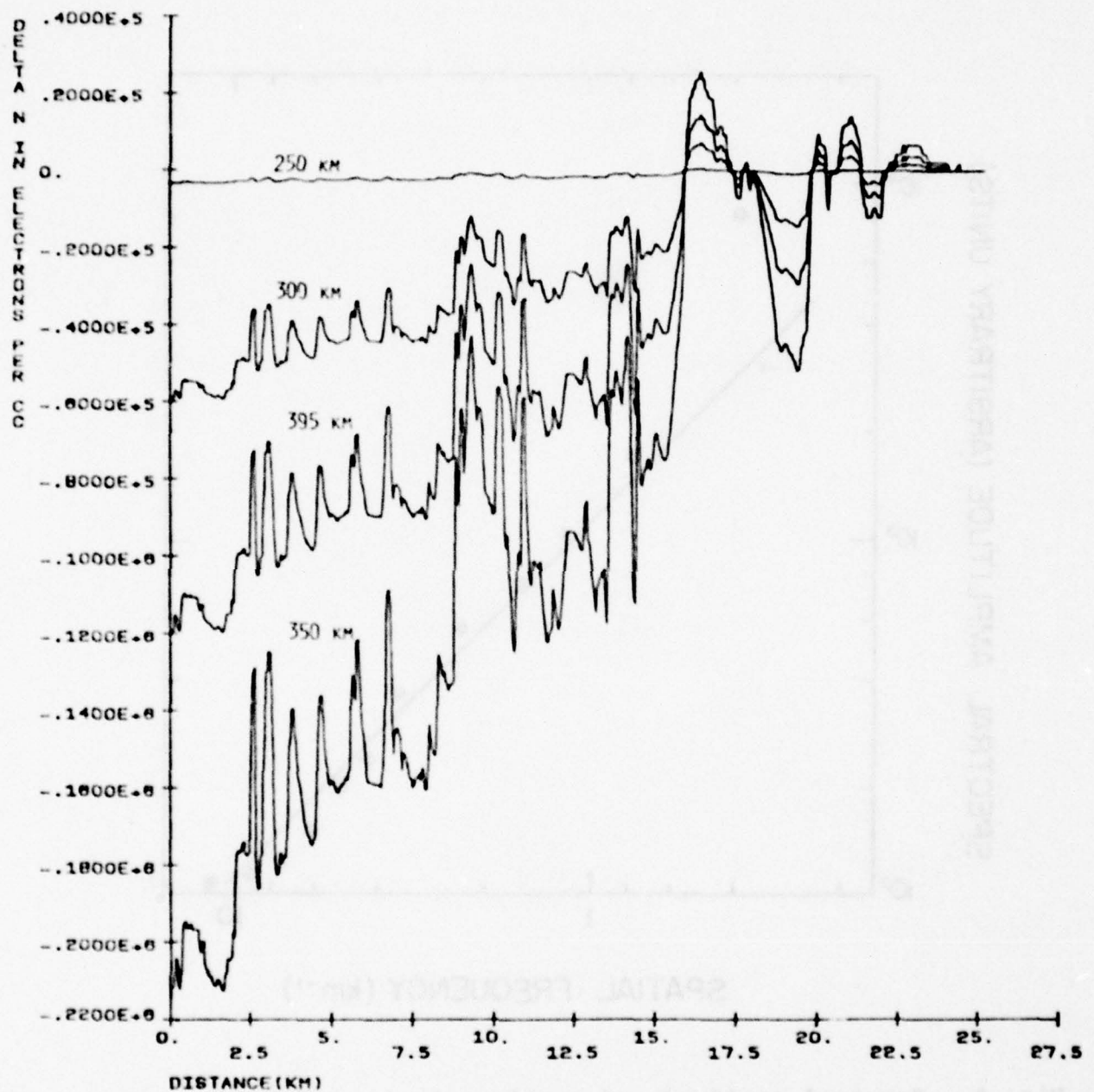


Fig. 4B. Horizontal electron density fluctuation profiles at different heights inside a plasma bubble, "developed stage."

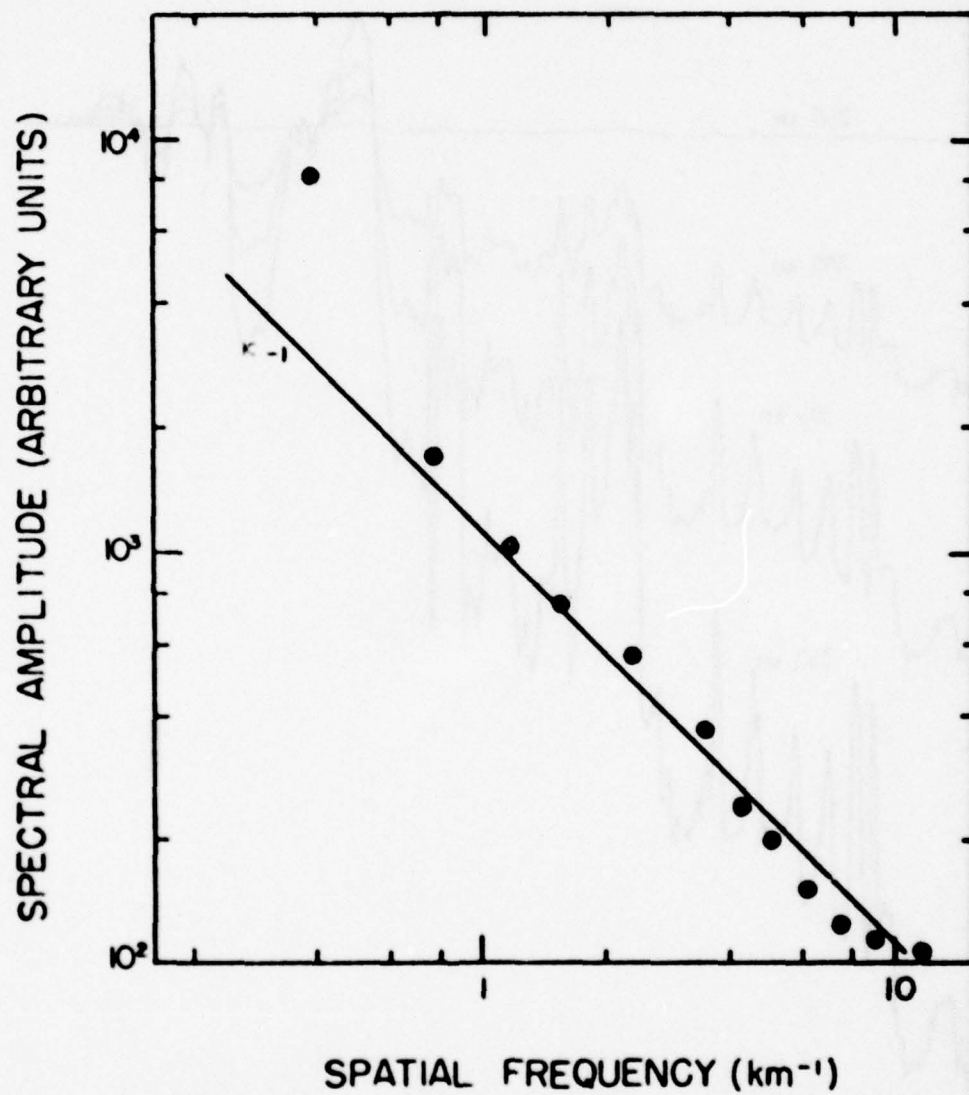


Fig. 5. Spectral amplitude of small-scale irregularities.

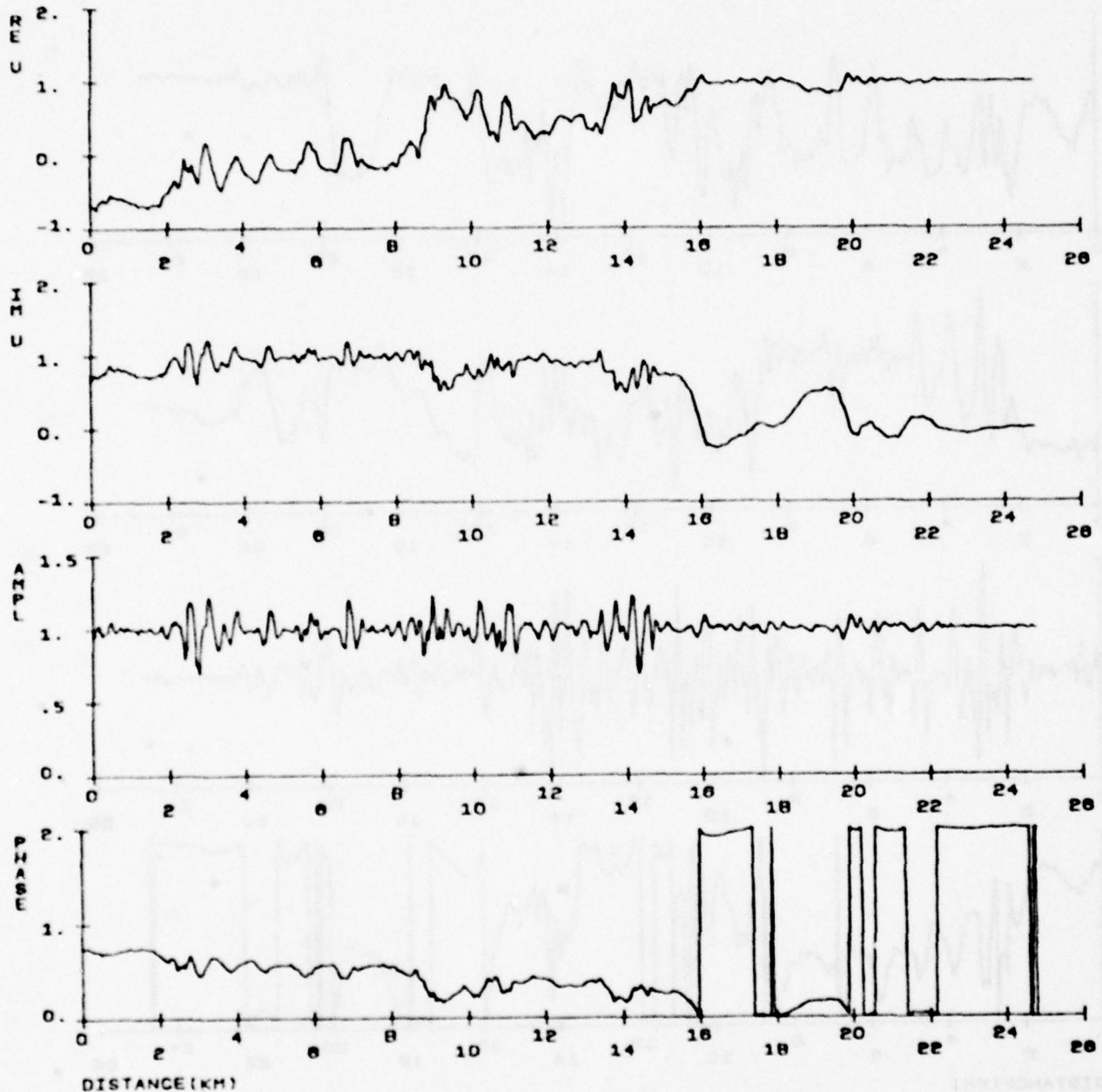


Fig. 6. Plots of the real and imaginary components of the complex amplitude, amplitude and phase (in  $\pi$  units) of a wave passing through the initial stage bubble and received on the ground. The wave frequency is 1500 MHz. Distance is measured from the projection of the center of the bubble on the ground.

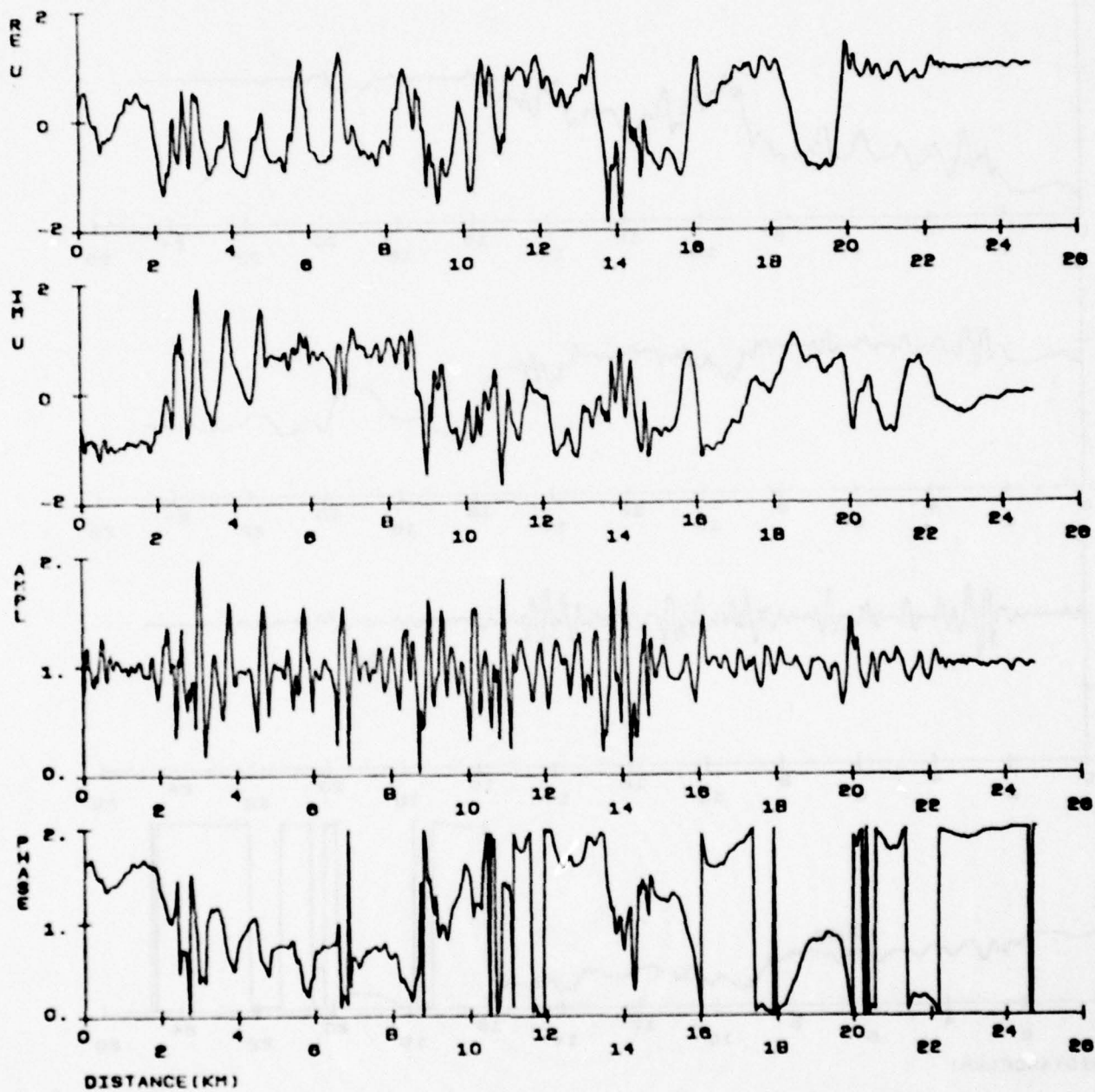


Fig. 7. Same as in Figure 6 but for the bubble in the developed stage.

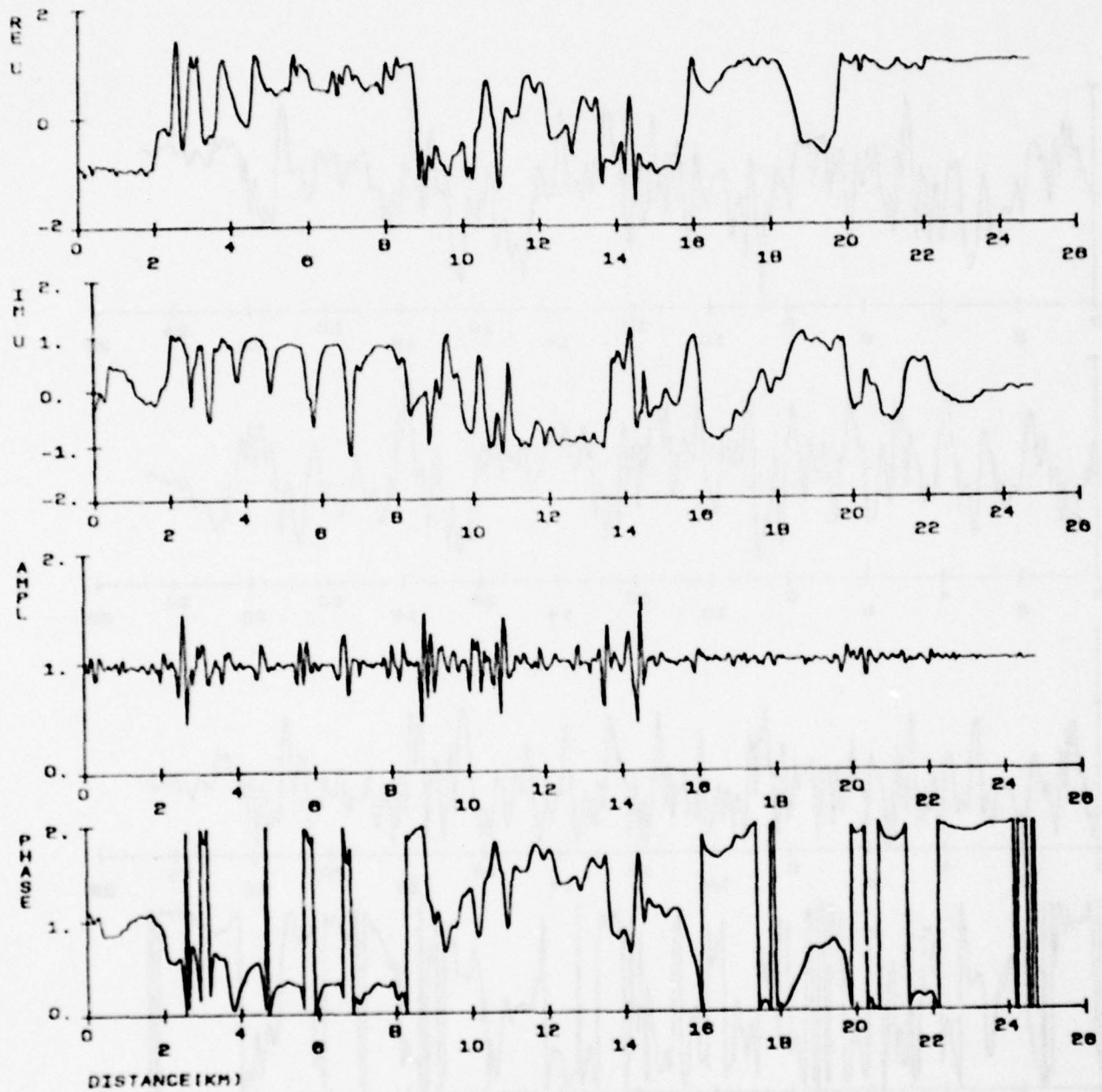


Fig. 8A. The same plots as in Figure 6 but at 136 MHz frequency. The wave structure at 300 km height is given.

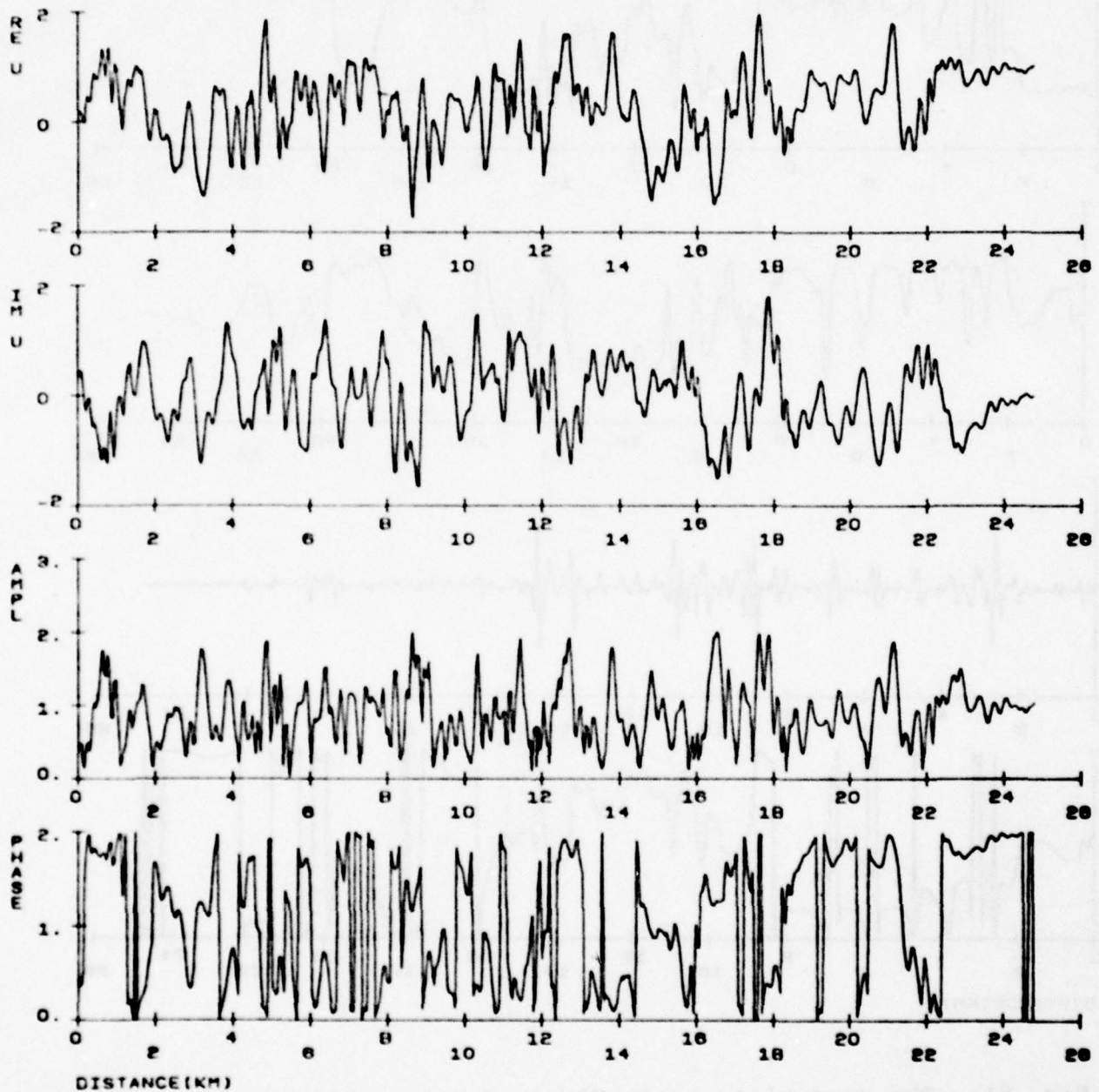


Fig. 8B. The same plots as in Figure 6 but at 136 MHz frequency. The wave structure on the ground is given.

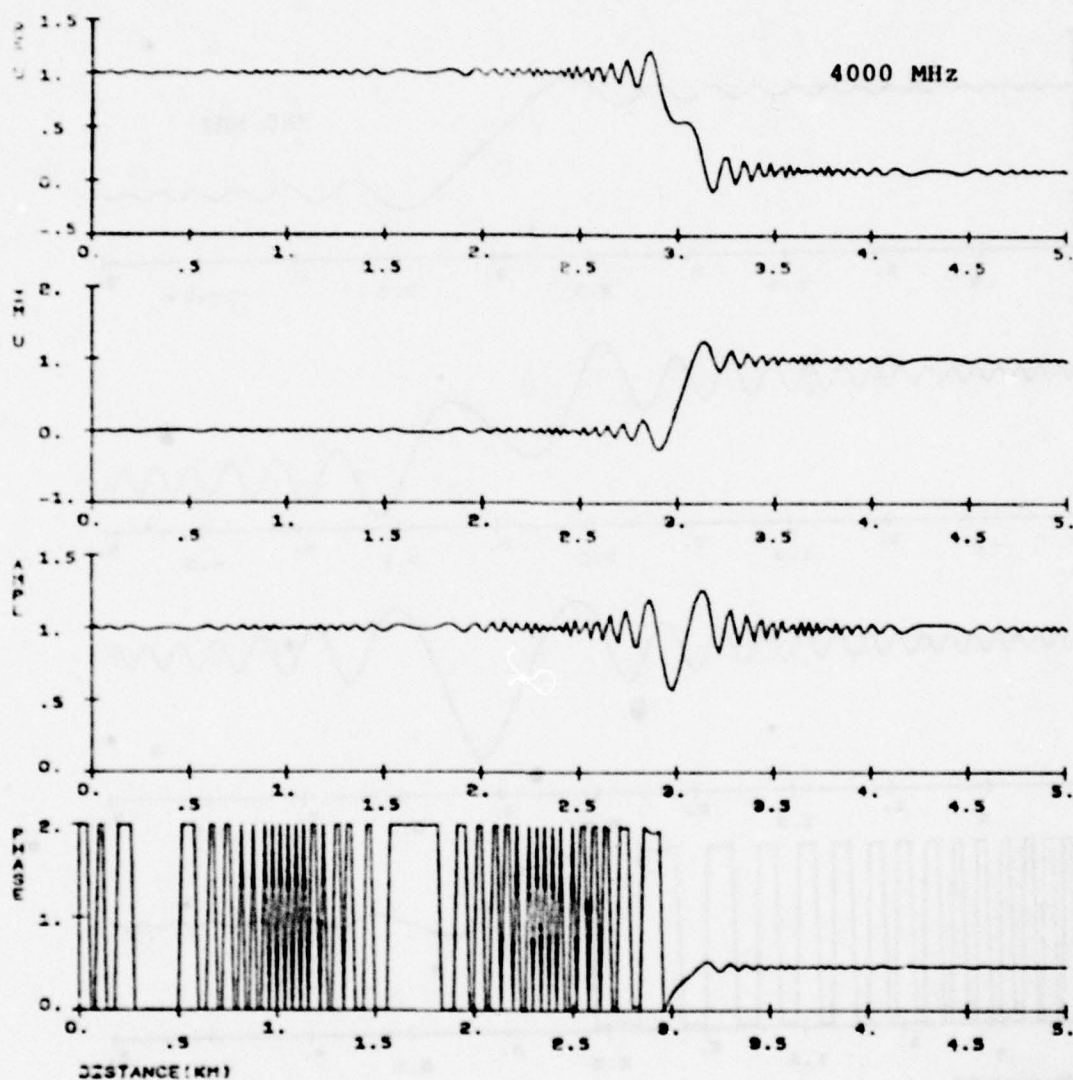


Fig. 9A. Wave structure after passing through a phase screen with discontinuity at a distance of 3 km. The phase screen height is 350 km at 4000 MHz.

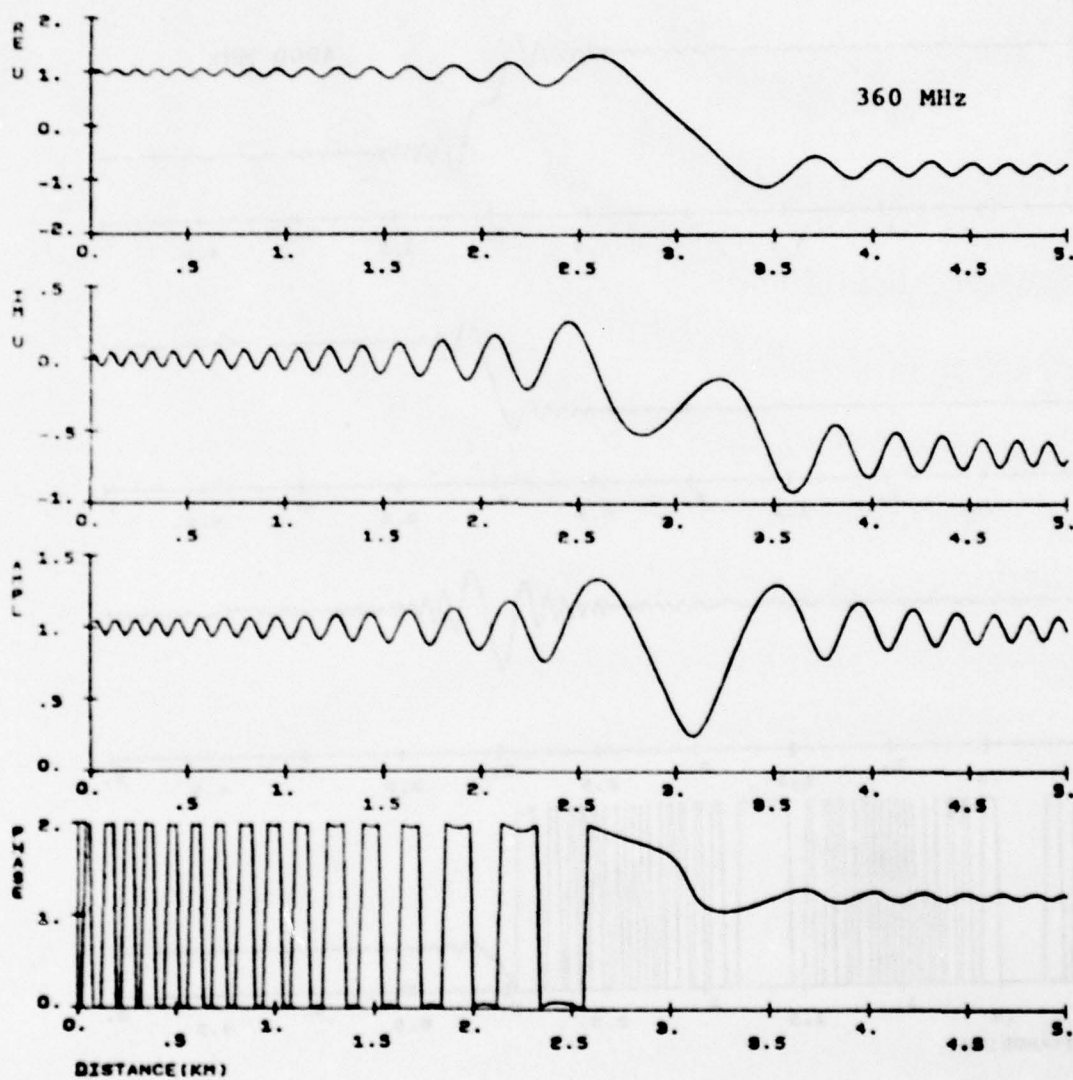
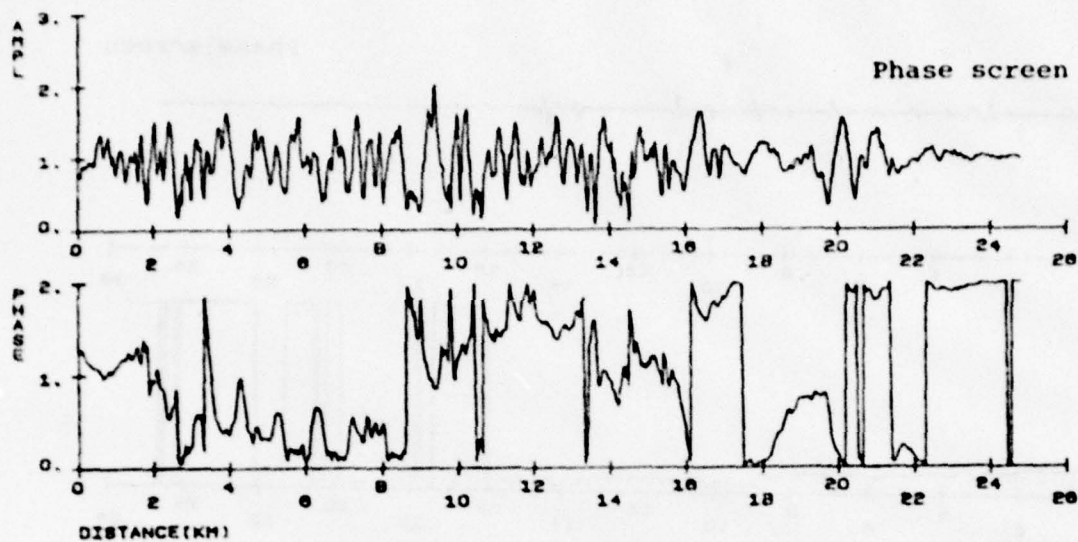
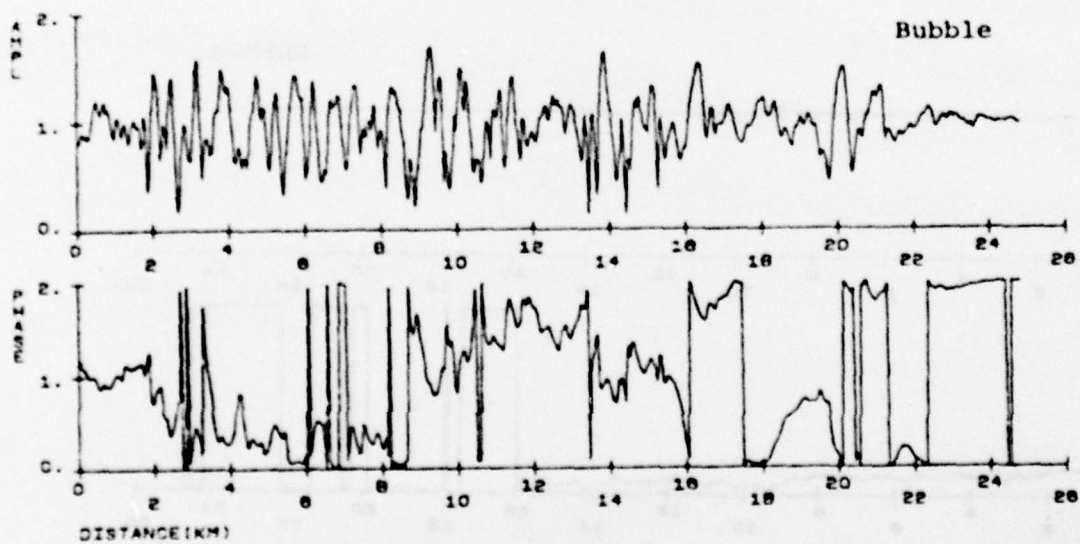


Fig. 9B. Wave structure after passing through a phase screen with discontinuity at a distance 3 km. The phase screen height is 350 km at 360 MHz.

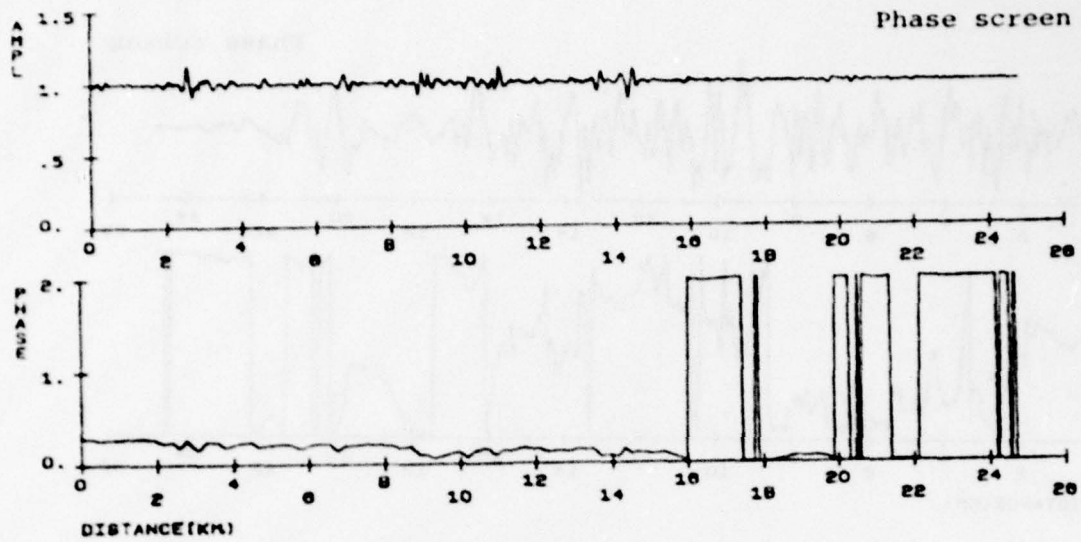


a)

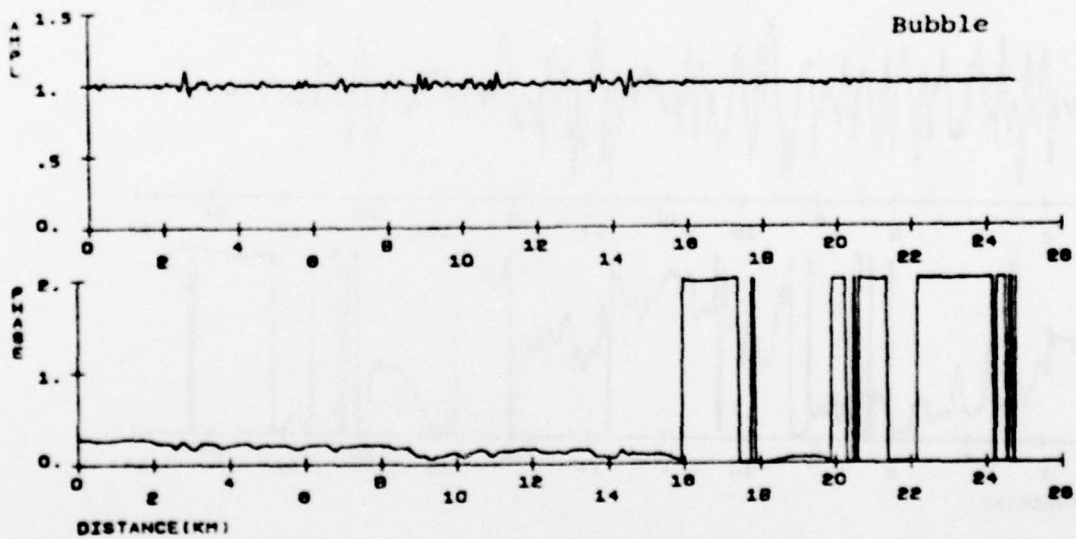


b)

Fig. 10. Comparison of the amplitude and phase pattern at 360 MHz produced by a) a phase screen and b) a bubble.



a)



b)

Fig. 11. The same as in Figure 10 but at 4000 MHz frequency.

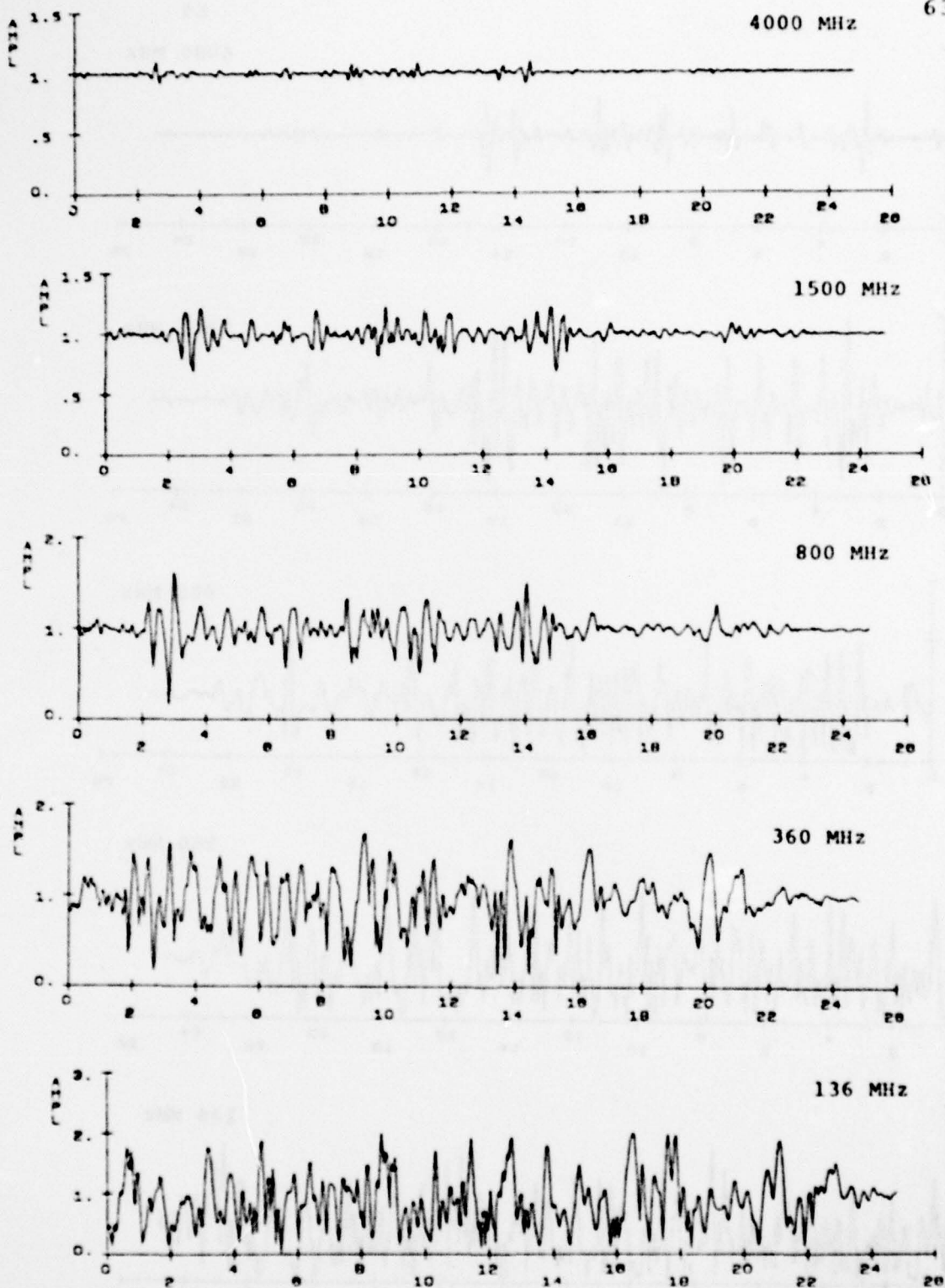
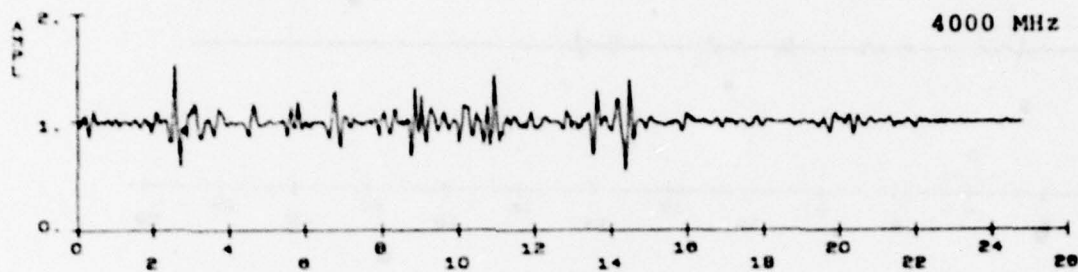


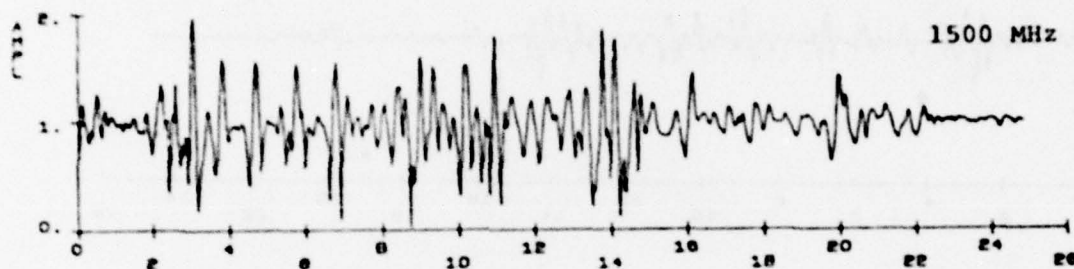
Fig. 12. Amplitude pattern at different frequencies produced by the "initial stage" bubble.

64

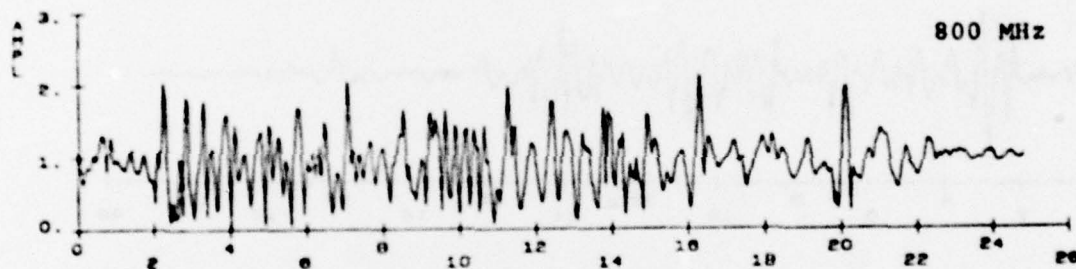
4000 MHz



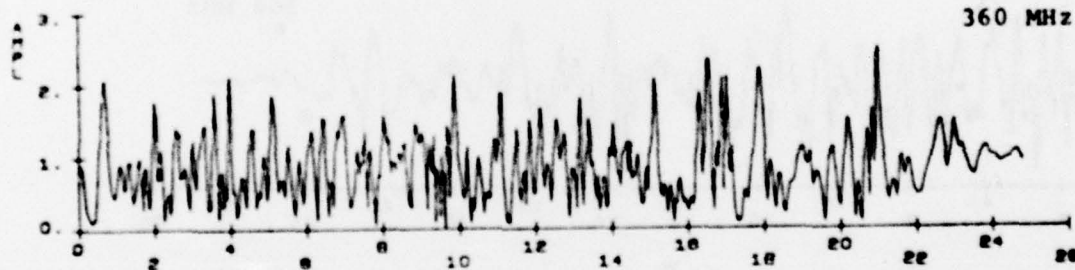
1500 MHz



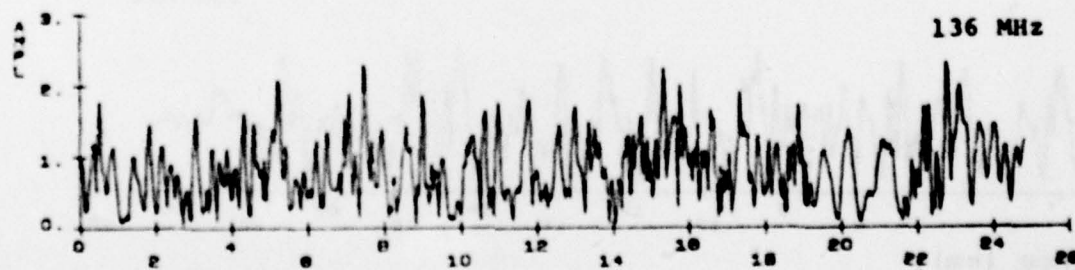
800 MHz



360 MHz



136 MHz



Distance (km)

Fig. 13. The same as in Figure 12 but for the "developed stage" bubble.

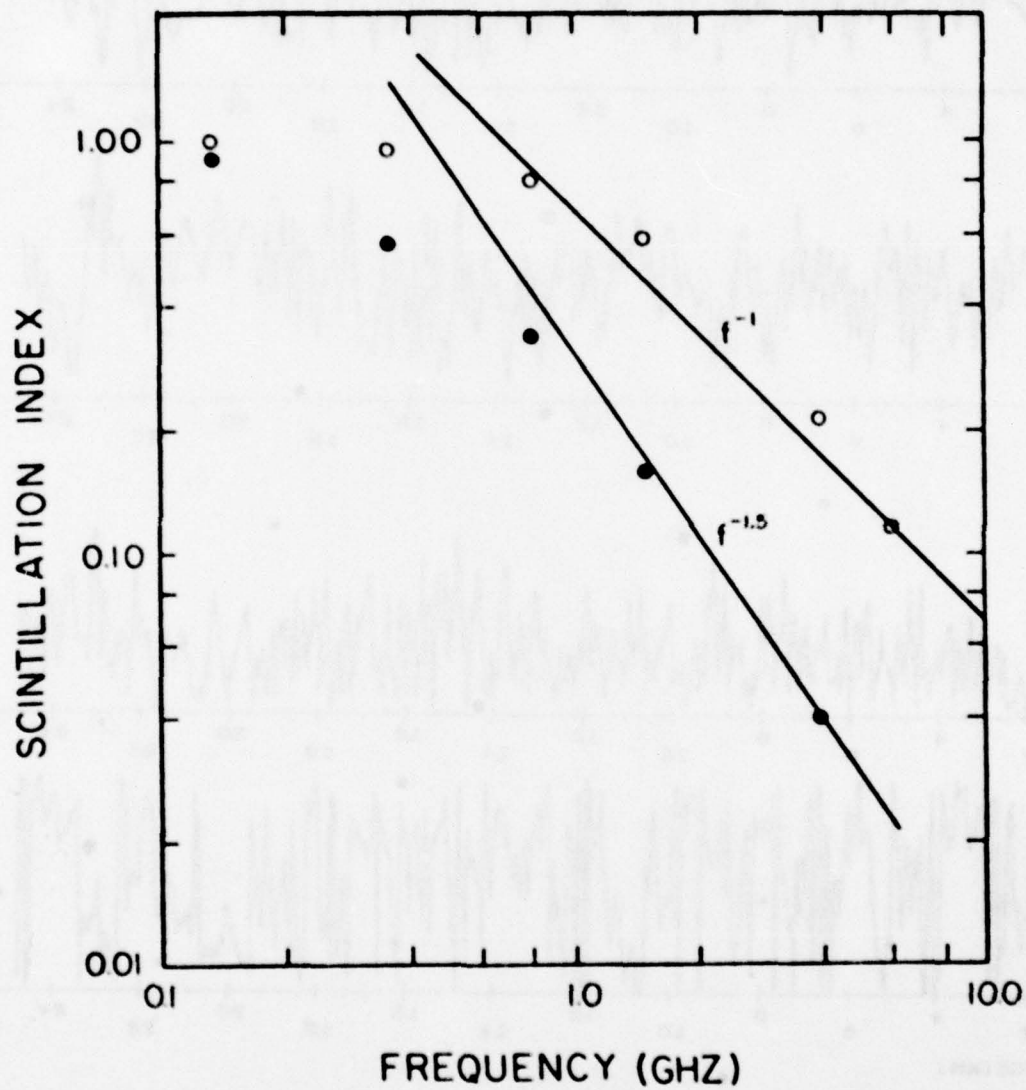


Fig. 14. Scintillation index frequency dependence for the "initial" (dots) and "developed" (open circles) bubble stage.

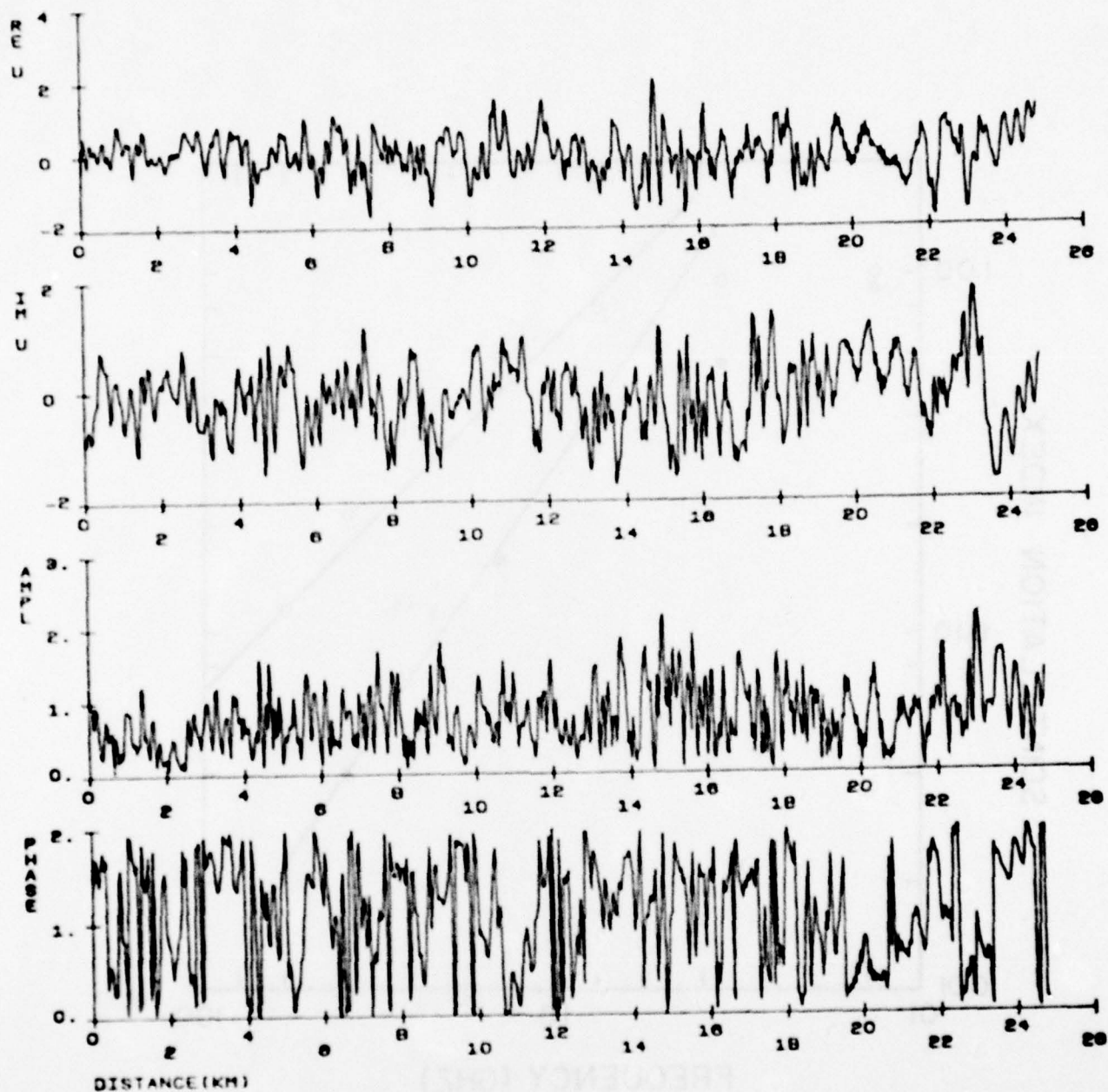


Fig. 15. Wave structure at 136 MHz produced by strong irregularities. Note lower level of the signal close to the center of the bubble.

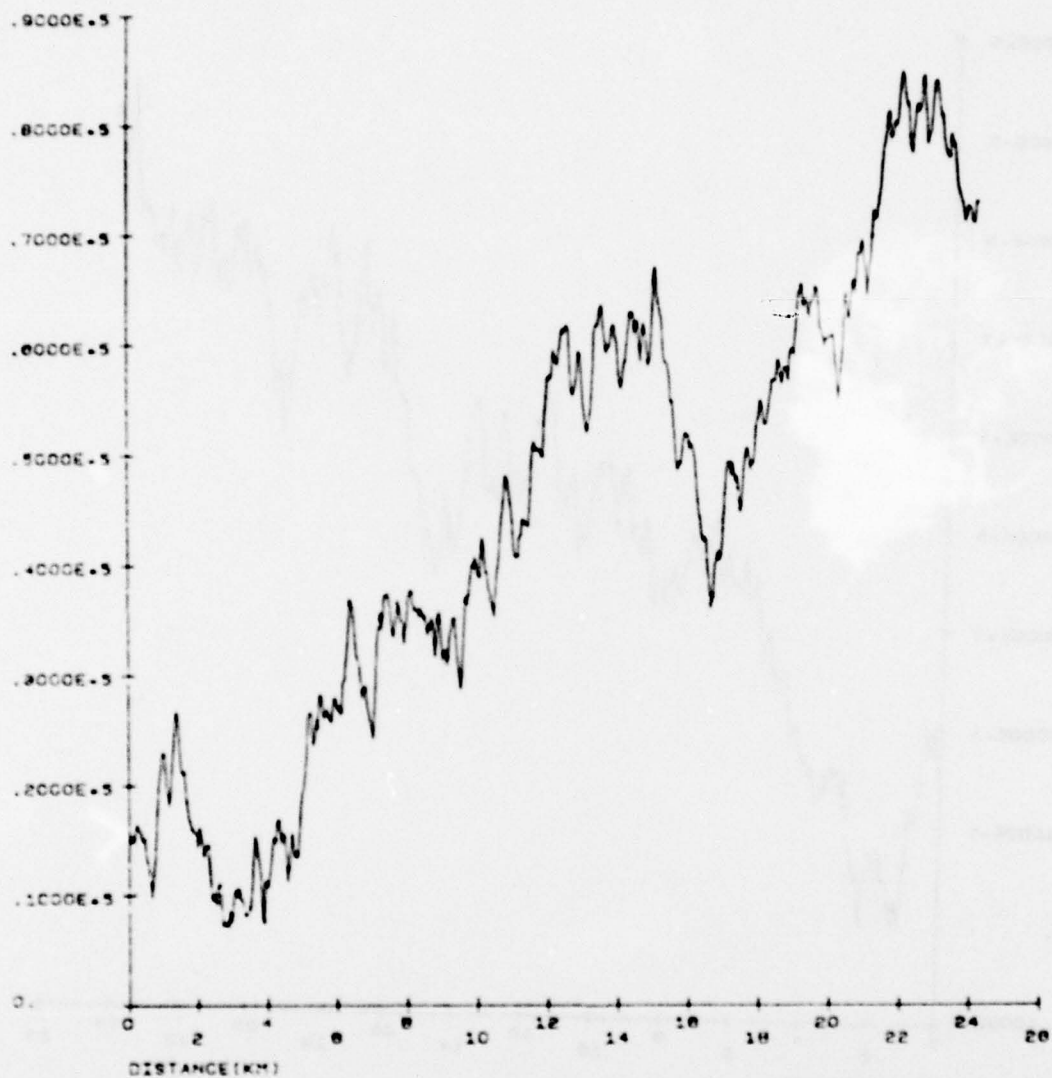


Fig. 16A. Horizontal electron density variations obtained by randomizing phases of the Fourier analyzed high frequency component of the data shown in Figure 1. Run A.

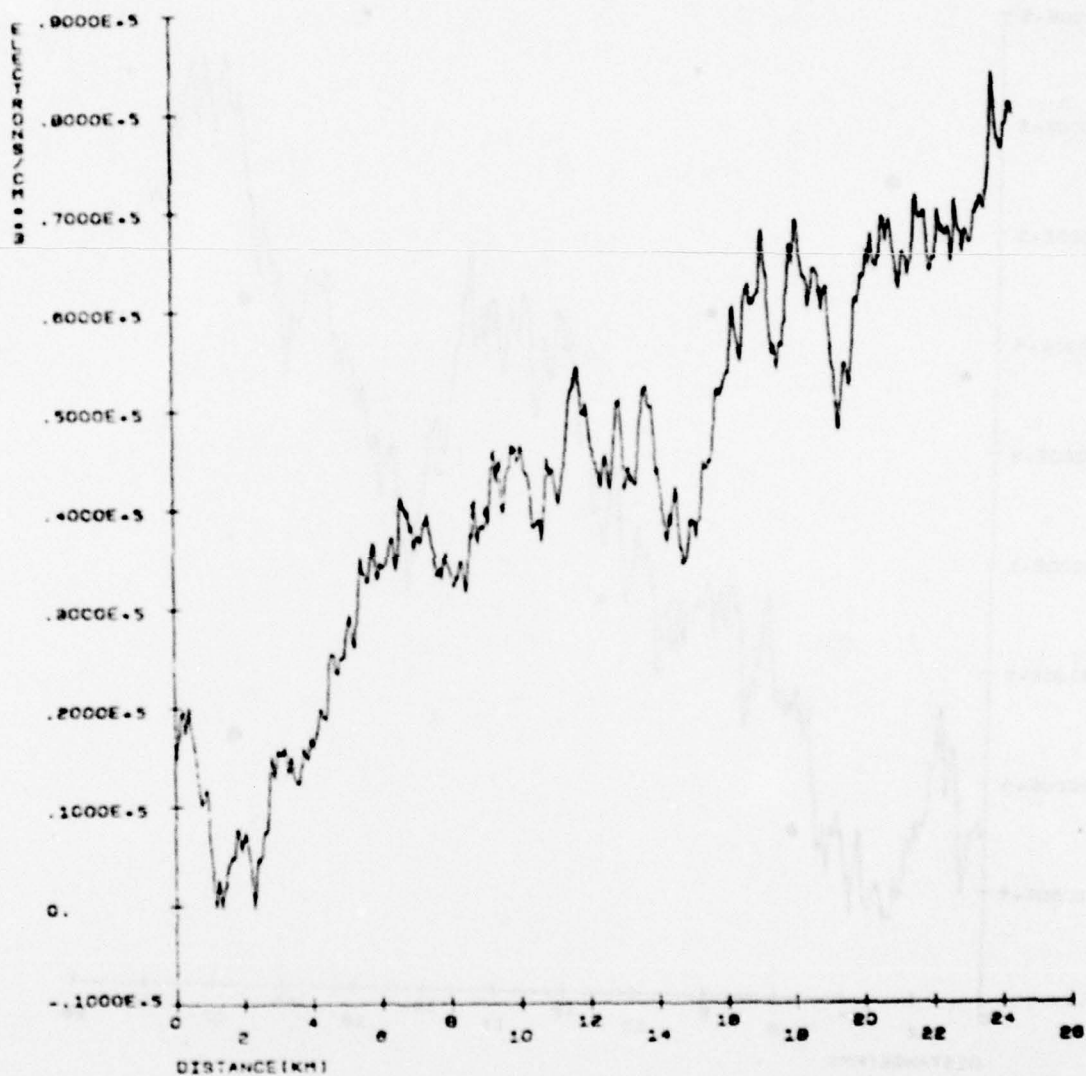


Fig. 16B. Horizontal electron density variations obtained by randomizing phases of the Fourier analyzed high frequency component of the data shown in Figure 1. Run B.

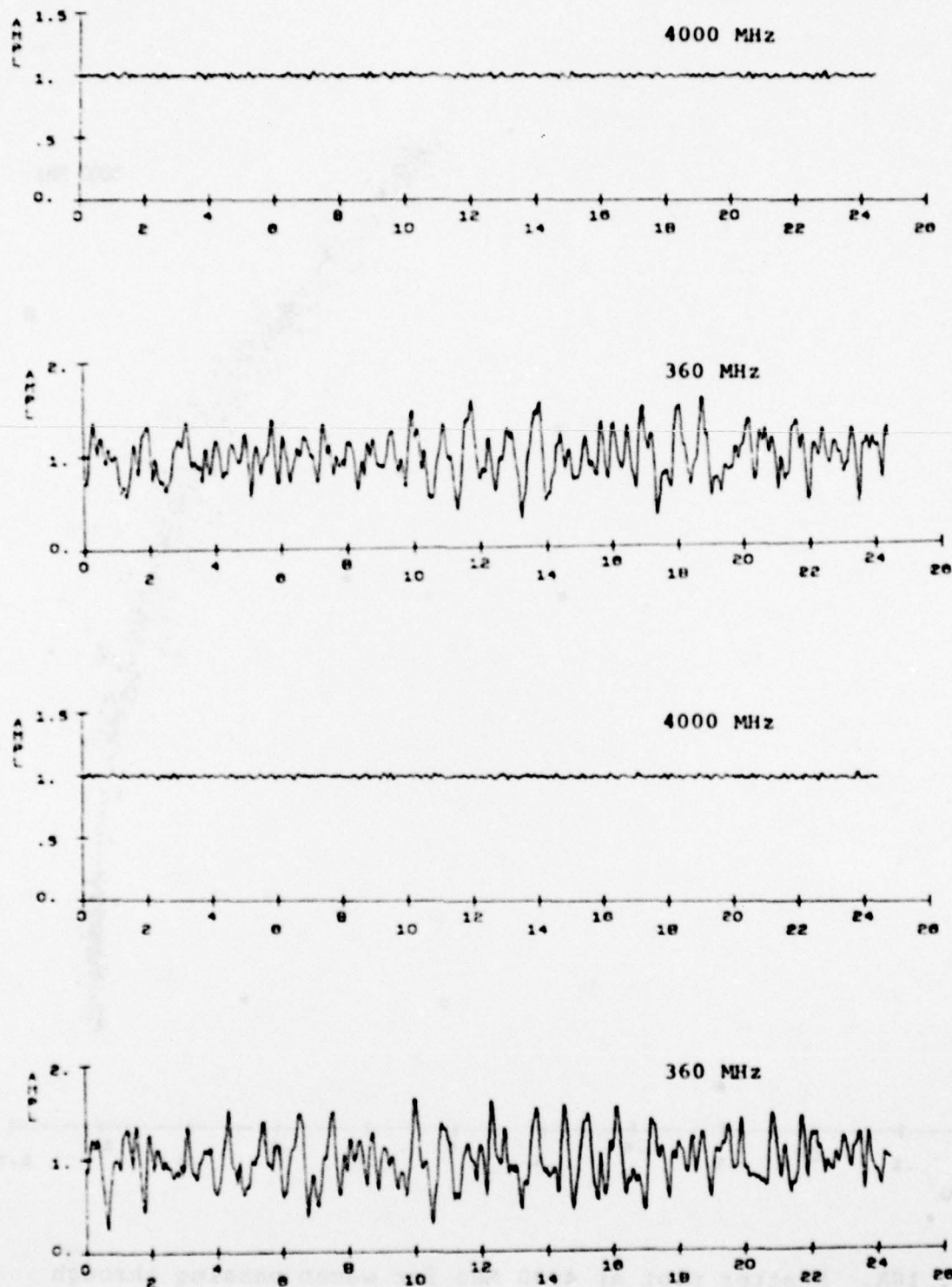


Fig. 17. Amplitude scintillation pattern at 360 MHz and 4000 MHz produced by the "initial stage" bubble with the horizontal structure shown in Figure 16. Two upper panels correspond to run A and two lower panels to run B.

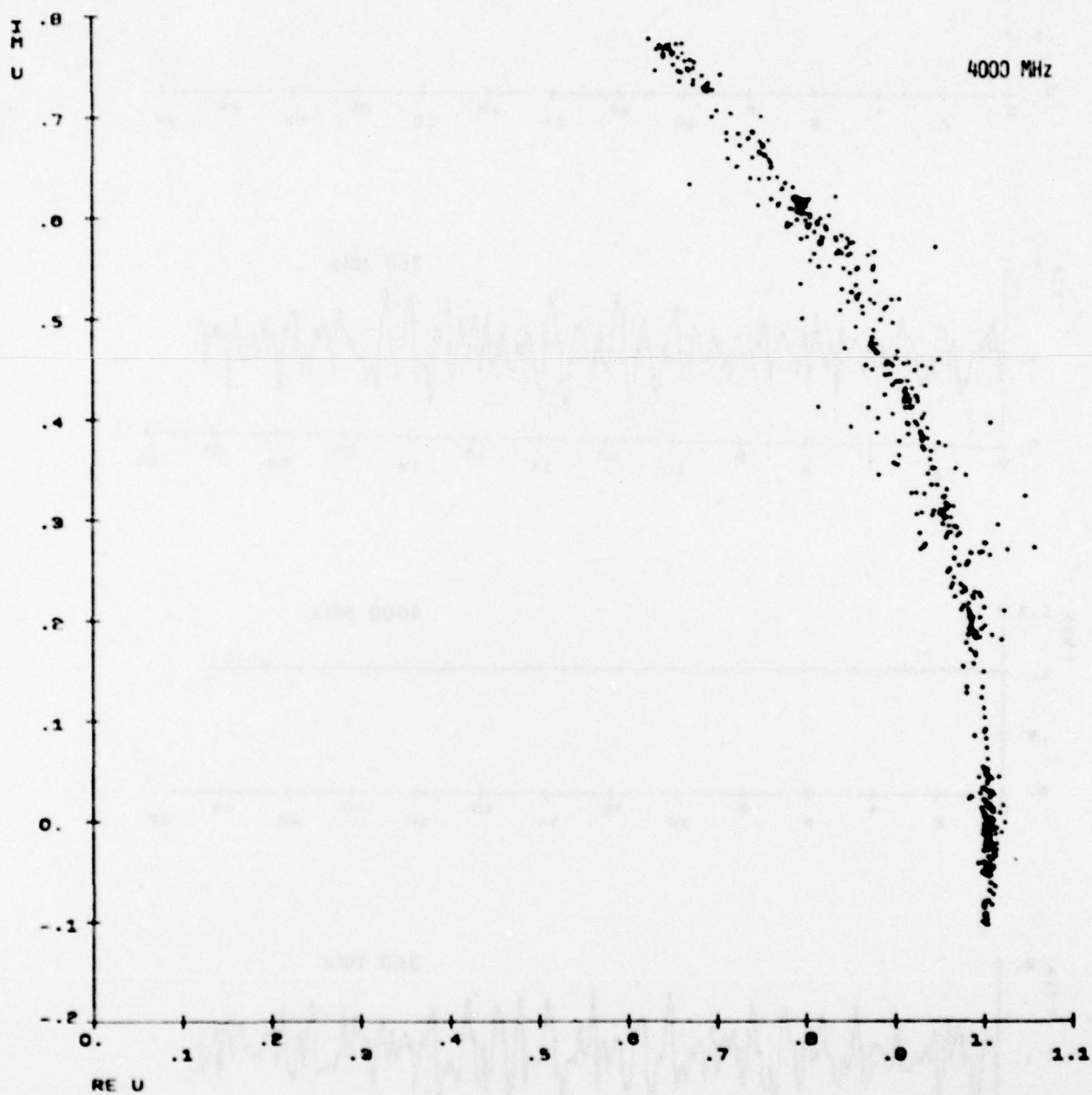


Fig. 18A. Scatter plot at 4000 MHz for waves passing through the "initial stage" bubble.

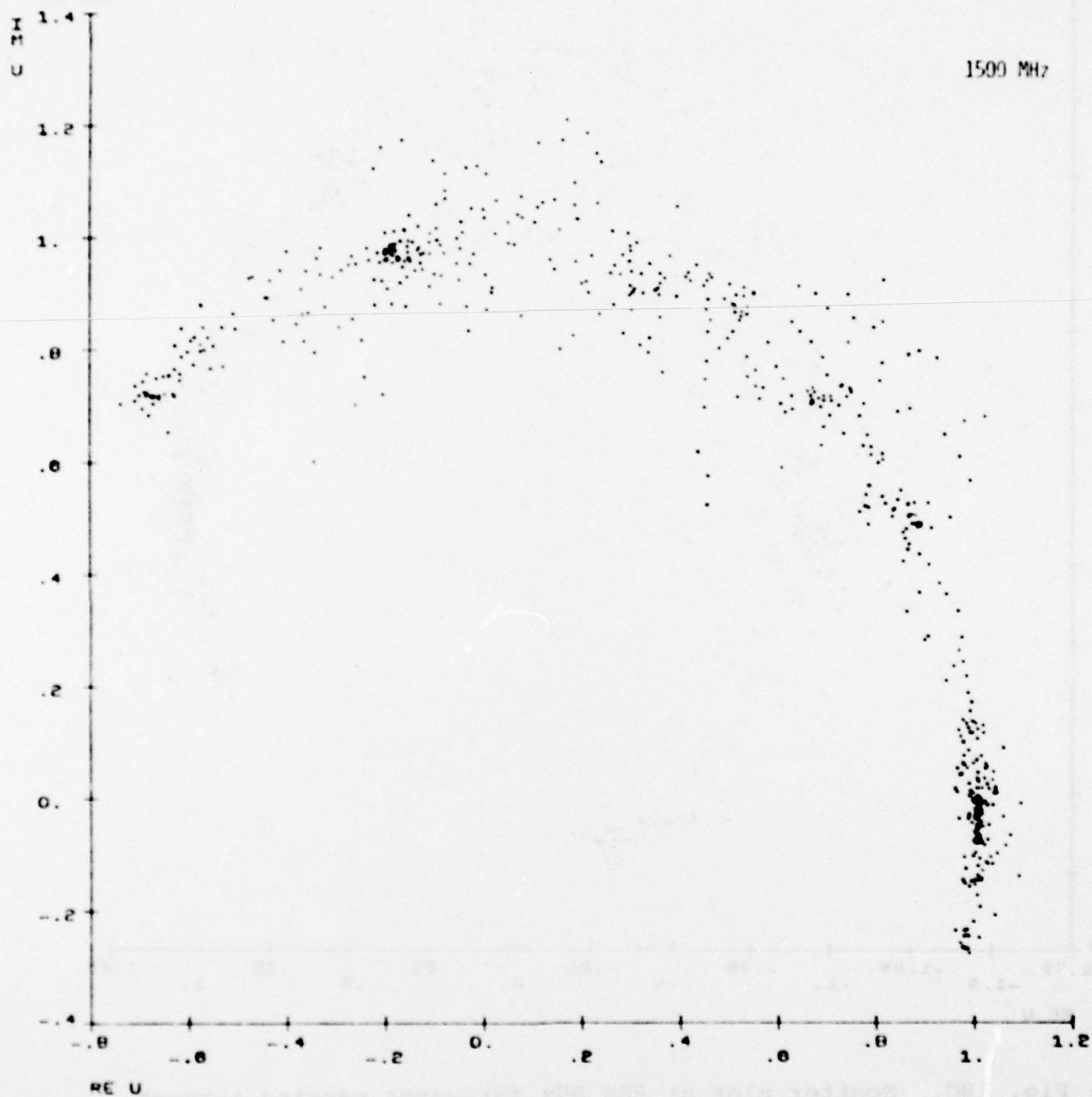


Fig. 18B. Scatter plot at 1500 MHz for waves passing through the "initial stage" bubble.

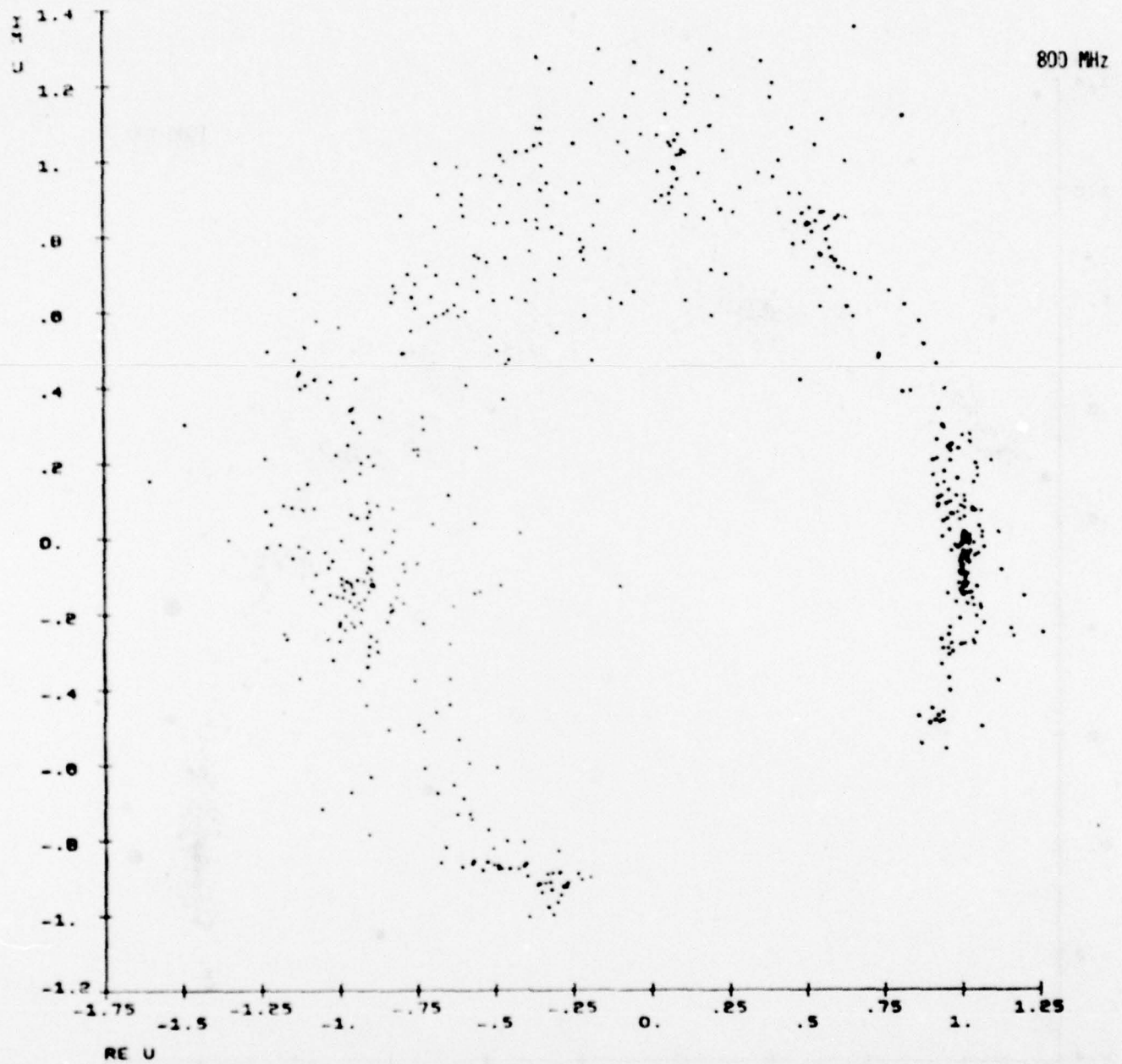


Fig. 18C. Scatter plot at 800 MHz for waves passing through the "initial stage" bubble.

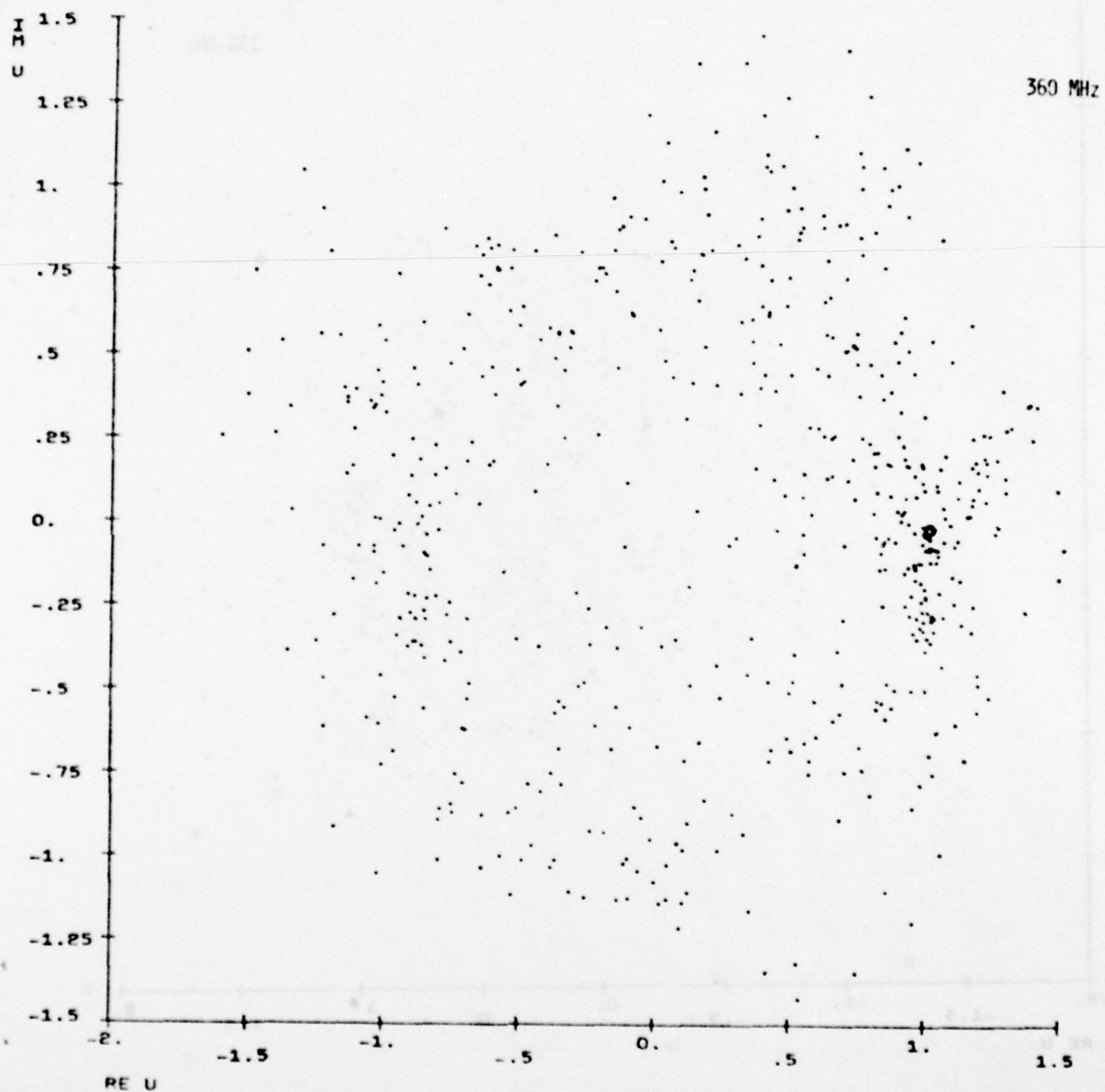


Fig. 18D. Scatter plot at 360 MHz for waves passing through the "initial stage" bubble.

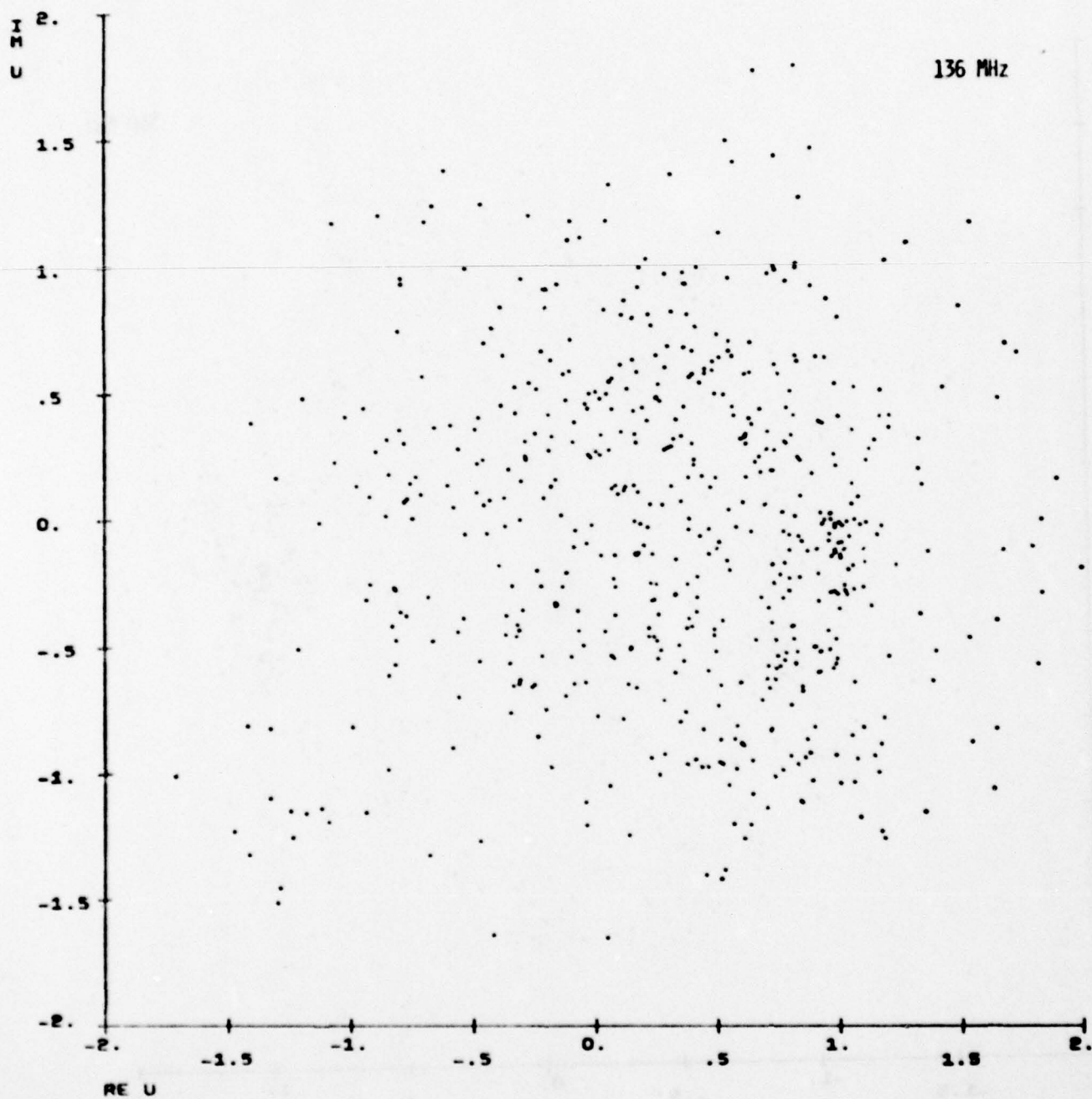


Fig. 18E. Scatter plot at 136 MHz for waves passing through the "initial stage" bubble.